Prototyping of an Automated Tip Lowering Mechanism for an Atomic Force Microscope

Submitted to:

Barbara Groh, Ph.D. Student
Walker Department of Mechanical Engineering
Austin, Texas

Prepared by:

Francisco Lara
Zoe Meyer, Team Leader
Christian Torres
Steven Yeung

Mechanical Engineering Design Projects Program
The University of Texas at Austin
Austin, Texas

Spring 2023

Prototyping of an Automated Tip Lowering Mechanism for an Atomic Force Microscope

Submitted to:

Barbara Groh, Ph.D. Student
Walker Department of Mechanical Engineering
Austin, Texas

Prepared by:

Francisco Lara
Zoe Meyer, Team Leader
Christian Torres
Steven Yeung

Mechanical Engineering Design Projects Program
The University of Texas at Austin
Austin, Texas

Spring 2023

ACKNOWLEDGMENTS

UTME AFM would like to thank our teaching assistant (TA), sponsor, and faculty advisor for their continued support and guidance throughout this project. Our TA, Nathaniel Heathman, was integral to the completion of this project, providing us with the support necessary to stay on-track with our project during the semester. Our sponsor, Barbara Groh, was of immeasurable help, aiding us in our learning of advanced mechatronics principles and LabVIEW programming. We would also like to thank our faculty advisor, Dr. Michael Cullinan, for taking the time every week to share valuable knowledge about precise actuation and machine elements, and for answering all of the questions we had throughout the duration of our project.

Furthermore, we would like to thank Jamie Svrcek and Ezekiel Moreno for their guidance in the machine shop and for supporting us during the hours of machining this project entailed. Finally, we would like to thank all of the graduate students in Dr. Cullinan's group for their kindness and helpfulness while we worked to complete this project–the lab was certainly a more welcoming place because of them.

Table of Contents

List of Figures

List of Tables

EXECUTIVE SUMMARY

Barbara Groh is working as a graduate student in Dr. Michael Cullinan's lab, focusing on the metrology of roll-to-roll (R2R) manufactured nanomaterials. To aid in her research efforts and maximize time efficiency, she is interested in optimizing her current, manual atomic force microscope (AFM) stand to automatically lower the AFM probe onto the nanomaterial specimen surface for scanning. UTME AFM is supporting this effort by designing, prototyping, and testing a working AFM stand with integrated automatic tip-lowering functionality.

The team identified the need to lower the AFM tip at a resolution of 0.1 μm, while limiting the lowering time to less than three (3) minutes and eliminating excess vibration produced by the device. This led the team to develop a two-step lowering process, using a servo motor on a ball-screw linear stage for coarse movement of the AFM towards the specimen and a voice coil and flexure system combination for fine motion of the specimen up to the AFM tip. The coarse motion phase will lower the total time of calibration while the fine motion phase will provide the precision and accuracy necessary to properly lower the AFM tip onto the specimen without damage to the AFM or specimen.

The team also outlined a control system for both movement steps using LabVIEW and the National Instruments' myRIO-1900, allowing the tip-lowering device to run off a single program. Operating both the ball-screw and voice coil using the same program allows the system to interact between the two phases of movement and limits the risk of incorrect timing and collision.

1 BACKGROUND INFORMATION

1.1 Sponsor Background

The sponsor for this project is the University of Texas Walker Department of Mechanical Engineering. The sponsor contact for this project is Barbara Groh; a PhD student in the University of Texas at Austin Walker Department of Mechanical Engineering. The primary focus of her research involves "photoelastic stress mapping for dynamic roll-to-roll metrology" ("Barbara Groh," n.d). The goal of this research is to assess the structure and properties of nanomaterials that are manufactured on a roll-to-roll mechanism through the use of an atomic force microscope (AFM). Overseeing Barbara Groh's research and also serving as our team's faculty advisor is Dr. Michael Cullinan whose research "focuses on the development of novel nanomanufacturing systems" ("Dr. Michael Cullinan," n.d).

1.2 AFM Team Background

The AFM team is composed of four senior mechanical engineering students who have worked together previously on the development and successful prototyping of an autonomous instrument as part of the ME 366K: Design Methodology coursework at UT Austin. The individual members of the team include: Christian, who is experienced with computer aided graphics (CAD) and analytical analysis; Zoe, who has industry and laboratory experience in structural analysis, report writing, and test procedure documentation; Frank, who is experienced with electronics and coding; and Steven, who is experienced with coding. The team's previous collaboration experience, combined with each member's unique capabilities, will lead to the development of a successful solution to the problem at hand.

2 PROBLEM STATEMENT

An AFM is used for metrology studies of samples on the nanoscale, generating a topographical image of the specimen. Our sponsor is currently working on real-time in-line metrology in roll-to-roll (R2R) manufacturing. Currently on the UT Austin main campus, no R2R manufacturing device is capable of in-line metrology, necessitating the use of stationary AFM set-ups. Wafer-scale pieces of material manufactured via R2R manufacturing must be cut out and moved to a standalone AFM set-up, such as the one Barbara currently uses (Section 2.1), for metrology and verification of correct manufacturing processes. The current AFM stand Barbara uses to do these scans requires manual lowering of the AFM tip onto the sample. The goal of our project is to automate the AFM tip lowering mechanism to accurately and quickly move the AFM tip to the optimal position above the specimen for an accurate scan.

2.1 AFM Background

The primary functions of an AFM consist of generating topographic scans and taking force measurements to analyze a sample's mechanical properties and structure.

The AFM setup currently being used by our sponsor is functionally identical to the schematic shown in Figure 1 with the notable difference being that Figure 1 shows the sample being raised up to the AFM, while Barbara's current setup manually lowers the AFM onto the sample while the sample stage remains stationary.

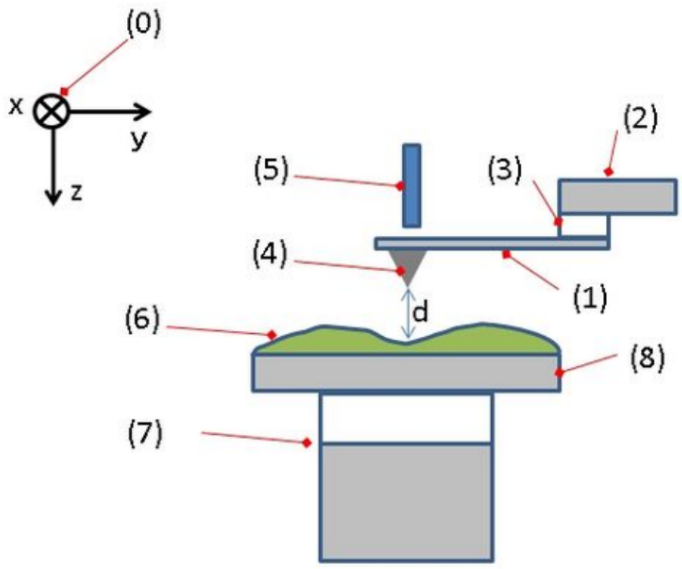

Figure 1. AFM setup. From *Typical Configuration of an AFM*, by T. Toyosaki, April 22, 2015 (https://en.wikipedia.org/wiki/Atomic_force_microscopy).

In Figure 1, the AFM itself is made up of a cantilever (1), support (2), piezoelectric element (3), tip (4), and sensor (5). The stage (7/8) raises the sample (6) to the tip of the AFM until they make contact (Toyosaki, 2015). As the tip runs along the sample, the cantilever deflects. The deflections are read by the sensor and are interpreted by software to generate topographic data.

The AFM can operate in three (3) different modes: contact, tapping, and non-contact. The contact mode can function in two separate ways: the first is by directly measuring cantilever deflection like the explanation for Figure 1. The second method relies on the use of a control system to maintain a constant cantilever deflection (Bullen, 2022). While contact mode produces scans quickly, it can potentially deform soft samples.

Tapping mode is less damaging to the material but has a slower scan speed than contact mode. In tapping mode, the AFM cantilever is driven to oscillate at its resonance frequency causing the AFM tip to interact with the sample at certain points. The deflection of the cantilever at these points can be used to generate a topographic image. In addition, as Van der Waals forces interact with the tip of the AFM, the oscillation of the AFM cantilever changes. This results in a phase difference between the driving and cantilever oscillations that can be used to determine the viscoelastic properties of the sample and produce a phase image (Etzler, 2012).

Non-contact mode is non-destructive but produces poorer resolution scans. Non-contact modes function by oscillating the AFM cantilever at a certain frequency. The Van der Waals forces between the AFM tip and sample surface change the frequency and amplitude of oscillation of the cantilever. A control mechanism adjusts the vertical position of the AFM such that the cantilever frequency or amplitude of oscillation remains constant. These changes in vertical position can then be used to generate a topographic map of the sample surface (Bullen, 2022).

2.2 Atomic Force Microscope Current Setup

The current setup used by Barbara within her research can be seen in Figures 2&3. This setup will act as the baseline of our project, as we will be replicating it in terms of its functionality, but automating the manual components of this device. For clarity, the AFM that Barbara uses in her research is the ICSPI benchtop nGauge AFM-on-a-chip, and its function and specifications are further elaborated in ICSPI, 2022. This specific AFM chip is also pictured in Figure 3 below.

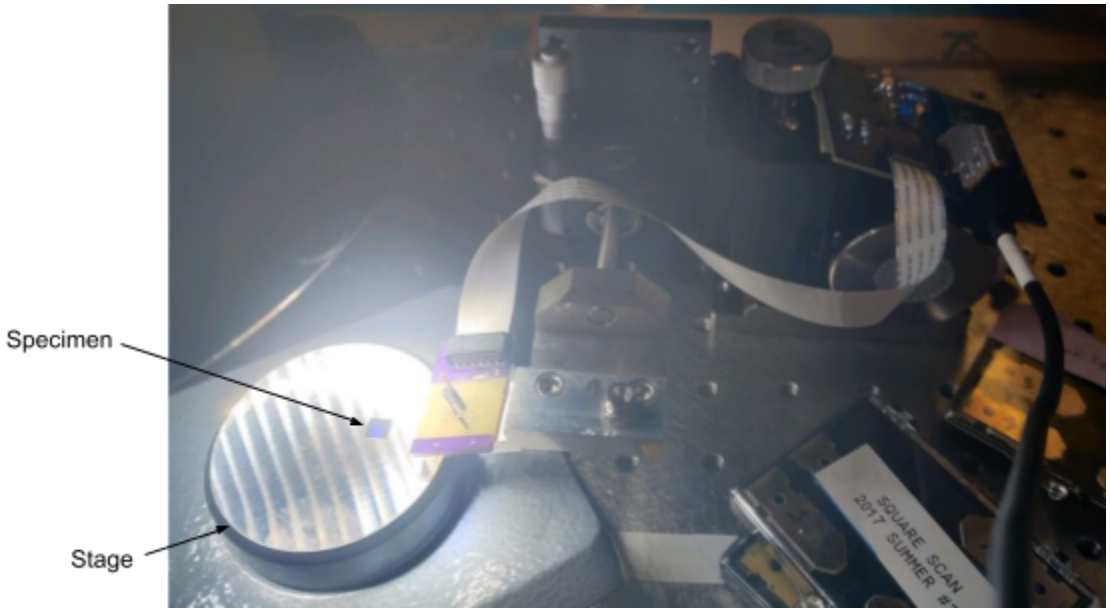

Figure 2. Current AFM setup overview

As seen in Figure 2, the specimen sits on a stationary stage independent of the AFM stand that sits to the right of the sample. Within Figure 2, one can see the yellow and purple circuit board that the AFM chip is screwed onto (see Figure 3). This board relays the information gathered by the AFM chip via the white cable to the second circuit board, which acts as an amplifier. This second AFM board itself is then connected to a microcontroller that serves as a DAQ. The DAQ is connected to a computer, where the nGauge software can read and interpret the data collected by the AFM. Note that all boards are accessible to the user in this current setup.

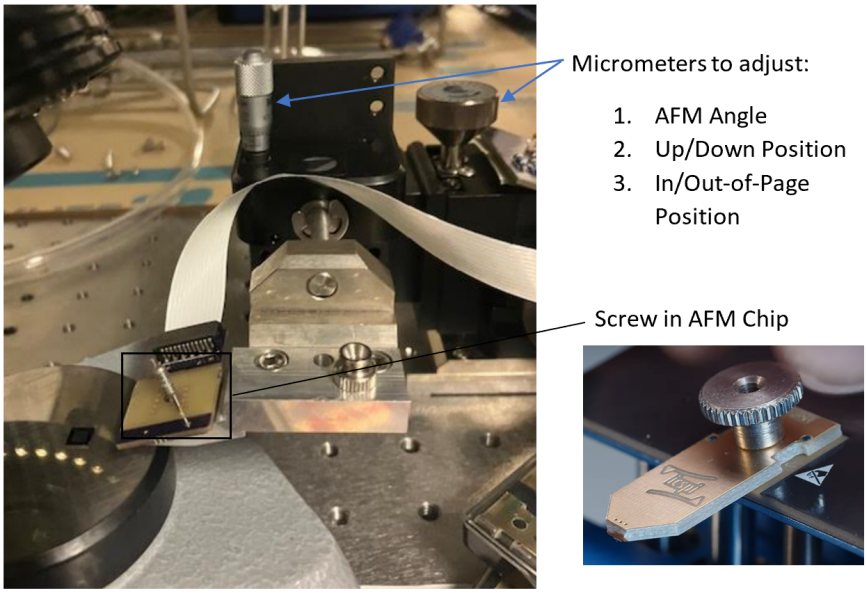

Figure 3. Labeled close-up of current AFM stand. Bottom right image from *Ngauge AFM*, by ICSPI, November 2, 2022 (https://www.icspicorp.com/ngauge/).

Referencing Figure 3, it can be seen that the current setup utilizes two (2) micrometer knobs which adjust, independently, the vertical and angular position of the AFM chip. The skinnier micrometer knob rotates the entire aluminum AFM stage via the axle running through the black micrometer stand. The larger micrometer knob moves the entire stage vertically towards or away from the specimen stage. The micrometer is positioned next to the stage such that the AFM lies above the sample. Using visual cues, the micrometer, and the nGauge software, the user manually adjusts the angle of the AFM tip to the appropriate angle for an accurate scan. To vertically position the AFM, the user manually turns the micrometer knob to approach the specimen. Once the AFM tip has adequately approached the specimen, the scan can be done.

2.3 Issues with Current Setup

Currently, there are a few issues facing the setup. Firstly, the position of the AFM has to be manually adjusted by turning the micrometer knobs. According to Barbara, adjusting the position of the AFM using the micrometer takes at least two (2) minutes. Since the micrometer lowers the AFM chip slowly due to its precision, it takes time to move the AFM close enough to the specimen for scanning.

Additionally, the user needs to monitor both the nGauge software and AFM chip visually as the position of the AFM is adjusted within the "entry region" of the specimen, which increases the odds of human error. As the AFM is fragile, these errors may lead to parts of the AFM breaking. For example, if lowered too much against the specimen, the tip of the AFM will break. If the tip breaks, the entire AFM is unusable, costing–on average–hundreds of dollars to replace the AFM chip.

Moreover, the current setup is also inaccessible to people with motor disabilities. To manually position the AFM, wrist and finger dexterity are necessary due to the fine twist motions required to adjust the micrometer knobs.

Furthermore, currently the user has to manually adjust the angular position of the AFM tip to an optimal angle for AFM tip lowering and scanning. At an angle where the AFM chip is too perpendicular to the specimen, the AFM tip may break off or damage the specimen during manual lowering. If the AFM is too parallel to the specimen, the AFM stage will hit the specimen before the AFM tip is in place, resulting in a failed AFM scan of the surface and possibly a damaged specimen.

2.4 Existing Solutions

Currently, ICSPI sells their own automated tip-lowering mechanism that is specifically built for their AFM-on-a-chip product, shown below in Figure 4 (ICSPI, 2022). While this market solution is a good reference in our team's design considerations, the product itself has a few issues that make it undesirable to our sponsor, even though they use ICSPI's nGauge AFM chips. Firstly, this device does not possess the desired Z-direction resolution necessary in Barbara's metrology, likely attributed to the use of a screw and rail system for movement. This system lacks precision, but also introduces friction that can be detrimental to the accuracy of the fine motion. Furthermore, the device itself is expensive. Given the amount of mechanical components readily available in Dr. Cullinan's lab and the machining and manufacturing resources our team has access to as UT Mechanical Engineering students, we are able to design and prototype our own version of an automatic tip-lowering mechanism for a relatively low cost.

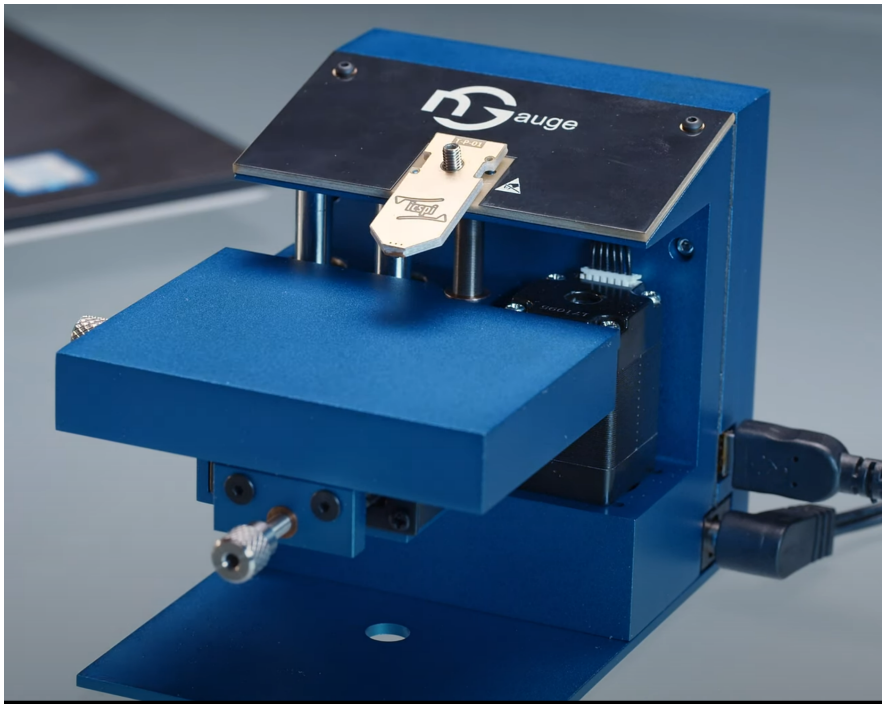

Figure 4. ICSPI Automated nGauge AFM Lowering Mechanism. Image from *Ngauge AFM*, by ICSPI, November 2, 2022 (https://www.icspicorp.com/ngauge/).

2.5 Problem Statement

Design and develop a functional prototype of an AFM stand equipped with an automated tip approach mechanism that shall be able to communicate with the nGauge software to verify the tip makes adequate contact with the specimen. Contact shall be made at the appropriate force and angle to ensure no damage to the AFM or specimen.

2.6 Deliverables

The deliverables for this project were outlined and discussed with our sponsor contact, Barbara Groh. The main deliverable is a functional prototype of an automatic AFM approach mechanism that adheres to the criteria listed in the specification sheet (Section 3). Along with the prototype, any code or CAD drawings or files utilized for the

final prototype will also be turned in so that the prototype may be replicated, repaired, or replaced in the future. Lastly, detailed documentation on the structure of the mechanism, how the mechanism functions, and any protocols on troubleshooting the mechanism will be delivered.

3 REQUIREMENTS & CONSTRAINTS

Table 1. Specification Sheet

Demand / Wish	Functional Requirements	Required Values/Targets	Units/Scale	Test/Verification Method
D	Accessible electronics			
D	Connect to computer			
D	Adequate approach without damage to AFM tip or specimen			
D	Robust enough to withstand handling loads	100	lb	
D	Input buttons	1-2		
D	Approach step size	0.1	µm	
D	Calibrates/is machined to proper AFM tip angle	15	°	Angle Measurement
W	Time to approach sample	< 3	min	Timer
D	Negligible vibration when not in use	0	Hz	Frequency sweep
W	Minimal/non-destructive vibration when in use			
Demand / Wish	**Constraints**	**Required Values/Targets**	**Units/Scale**	**Test/Verification Method**
		Size		
W	Comparable size to current setup	1x1x1	ft^3	Measurement
		Cost		
D	Up to twice that of current setup	3000-4000	$	

For our device, the AFM team aims to develop a device that meets requirements and constraints laid out by the sponsor contact and summarized in the specification sheet given above in Table 1. Firstly, all electronics and circuit boards must be easily accessible and replaceable, and the device must operate in conjunction with the nGauge software. As the measurements are on the micro- and nano- scale, the nGauge program is crucial for determining when the AFM tip has made adequate contact with the sample for measurement. The device should have no more than two input buttons for ease of user accessibility. The device should be able to set the tip of the AFM to an optimal angle to

avoid damage of the AFM and accuracy of measurements. The optimal angle to mount the AFM chip was determined to be 15° from the horizontal, as given by an engineer at ICSPI, the manufacturer of the nGauge AFM (Zhenle, personal communication, Feb. 15, 2023). This angle was also given in Yao, 2016, giving our team enough documentation to proceed with an optimal angle of 15°. The device should also approach the specimen sample with step sizes of 0.1 micrometers as the AFM tip enters the entry region of the specimen to ensure precision. The whole automated process should take under three (3) minutes as the current manual adjustment process requires at least two (2) minutes. Even if the device takes slightly longer than the targeted time, it still serves as a safer alternative to approach the specimen compared to performing the approach manually. By the end of the procedure, the AFM tip should make adequate contact with the sample without damaging the AFM tip or specimen. The device should also be robust enough to not break if it is properly handled.

Finally, vibrations produced by the device need to be minimized while on and off. It is essential to control the vibration of the device as it can affect the data collection considering how minute the measurements are. When the device is turned off, it should produce no measurable vibration as the entire laboratory is vibration sensitive. When the device is in use, it ideally operates under the noise floor of the optical tables used in the lab to isolate vibrations. Fortunately, vibrations during the device's use are not as detrimental as vibration of the device while it is locked, off, and the AFM is scanning. Qualitatively, vibration during tip lowering should be limited and non-destructive, meaning the vibrations should not affect the accuracy of the step sizes during fine motion

of the device, limiting the possibility of damage to the AFM tip by premature collision with the sample due to large vibrations.

The constraints of the device include a compact design that fits within a 1 ft x 1 ft x 1 ft space and a budget of $3000-$4000. The size constraints of the device can be expanded if needed but should be a comparable size to the current setup. The budget is approximately twice that of the current setup which the team found to be about $1500-$2000.

4 CONCEPT GENERATION

4.1 Functional Model

Before beginning the design process, we created an initial functional model to outline the possible subsystems of our device. The functional model is composed of six (6) subsystems and is shown below in Figure 5.

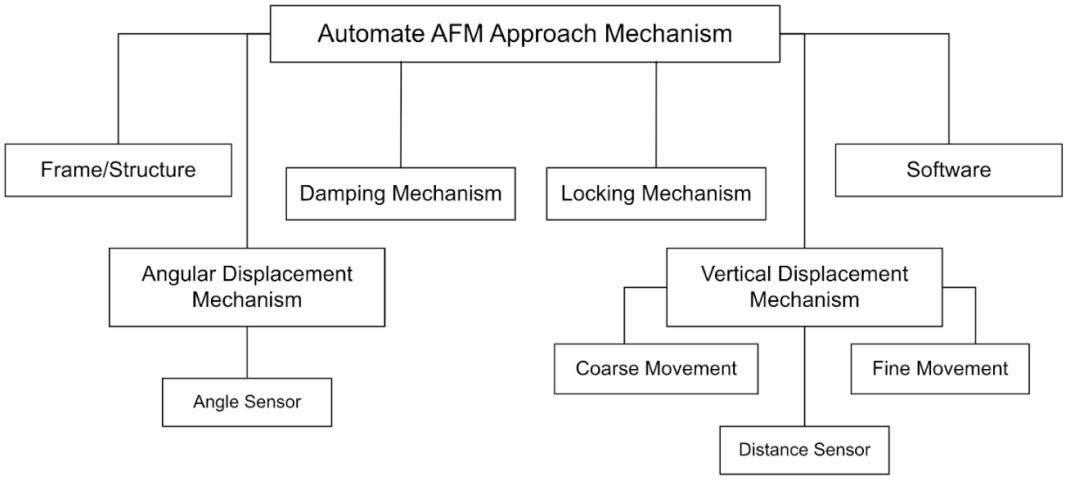

Figure 5. Functional Model for Automating an AFM Approach Mechanism.

The first subsystem, “frame/structure”, refers to the structure of the device itself. For our device, the structure itself must be rigid and house all required components for the device (i.e. structure is self-containing).

After analyzing our sponsor’s current setup, we established two displacement subsystems that enable angular and vertical movement. An angular displacement mechanism is required in the current setup to freely adjust the AFM tip to its optimal angle relative to the horizontal sample surface. Due to the automatic nature of our device, if a variable angle option was implemented, we would need to also consider the necessity of an angle sensor. The vertical displacement subsystem is further broken down into

mechanisms for coarse and fine movement, both of which require the consideration of distance sensors, to increase the amount of options available to us in terms of movement mechanisms.

As external vibrations influence the resulting scans the AFM generates, a damping subsystem may be required to minimize the device's vibrations during operation. In addition, an external locking subsystem may be required to lock the position of relevant device components once the AFM has successfully made contact with the sample. This would ensure that no further movement of either the AFM tip or the sample stage would occur during scanning, decreasing the possibility of collisions, tip damage, or inadequate scans.

Lastly, a crucial subsystem for our device is software. A computer program is necessary to control all automatic components of our device, including any possible angular or vertical displacement mechanisms or any automated locking devices.

4.2 Patent Search

Upon review of the literature and a thorough patent search, our team was not able to find any patents for automatic tip lowering mechanisms for AFM-on-a-chip type devices. The nGauge system we referenced to generate our double ball screw mechanism shown in Section 4.3 is also unpatented (ICSPI, 2022). Therefore, the relevant patents pertaining to our project center around mechanisms for low-vibration micropositioning.

One such patent, filed by Nanofactory Instruments AB, outlines a micropositioning device aimed for use in microscopy by utilizing piezoelectric tubes to accelerate and decelerate an object (Olin, H., 2003). The patent design showcased below in Figure 6 could potentially be modified to finely actuate a sample stage.

Figure 6. Micropositioning Device Patent. Image from *Micropositioning device,* by Olin, H., et. al., 2003 Patent.

Another patent, filed by UChicago Argonne, LLC, shows the use of flexure mechanisms in vertical nanopositioning. The vertical nanopositioning, shown in Figure 7, uses parallel flexure linear guiding mechanisms, further stiffened by a middle bar relative position control mechanism. Within the scope of this patent, the idea was to allow for a vertical displacement of the stage by 12-16mm under a load of 2-4kg, based on the needs of the scanning stage of an x-ray microscope (Shu D., et. al., 2020). This application of micro- and nano- precision sample stages for the use of metrology correlates well with our project, and the use of parallel linear flexure mechanisms with a specific driving mechanism can be called upon, modified, and used in the creation of our fine motion actuation.

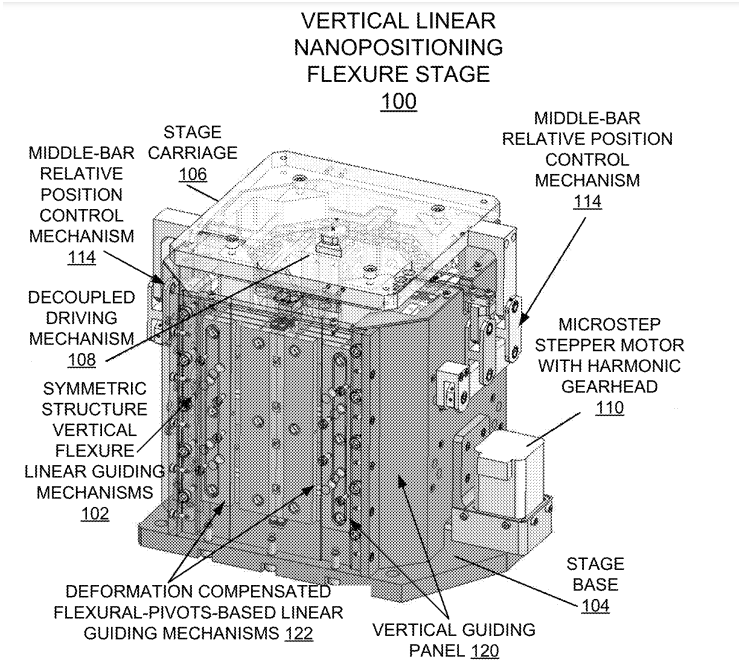

Figure 7. Vertical Linear Nanopositioning Flexure Stage. Image from Shu D., et. al., 2020 Patent.

The patent filed by Industrial Technology Research Institute (ITRI), shown in Figure 8 outlines a design that enables long-stroke displacement with resolution at the nanoscale. Like the patent shown in Olin, H., 2003, this patent also utilizes piezoelectric actuators to produce high resolution movement. The patent design is showcased below and functions along three (3) axes. In addition, the displacement of the piezoelectric tubes varies with the input voltage. In theory, this design can have a resolution of 0.1nm (Pan S-P., et. al, 2005).

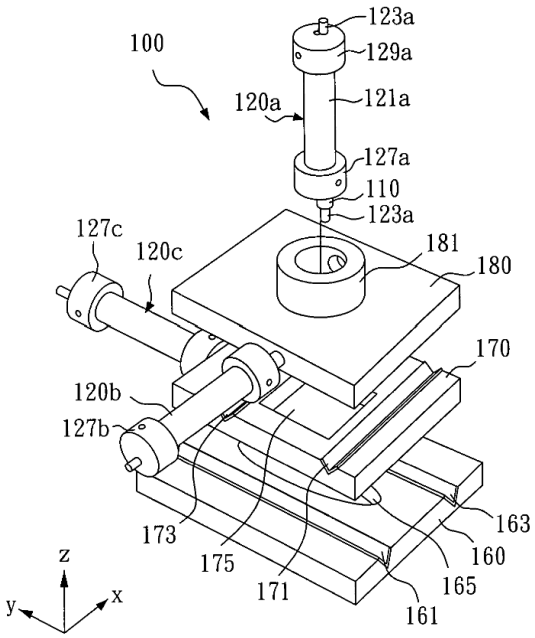

Figure 8. High Resolution Nanopositioning Mechanism Patent. Image from Pan, S-P., et. al., 2005 Patent.

4.3 Preliminary Decisions

To further simplify our design before concept generation, we decided to remove the need for an angular displacement mechanism as the optimal AFM angle has already been determined to be fifteen (15) degrees from horizontal as mentioned in Section 3. Therefore, the AFM stand may be machined to a stationary angle of 15°, eliminating the need for any angular calibration. Additionally, we decided to eliminate the need for distance sensors for both fine and coarse movement mechanisms as sensors introduce unnecessary cost and complexity.

For fine movement, the AFM piezoresistive sensors can function as pseudo-distance sensors as the AFM inherently uses voltage measurements to inform the nGauge software on how close the tip is to the sample. This can be utilized during the fine movement phase of vertical displacement, which will be further elaborated upon in Section 8 of this report. We also decided to utilize a linear precision ball-screw actuator for coarse movement which removes the need for an external coarse movement distance sensor as long as there is a defined distance for the ball-screw to lower. By defining a "home" position and a "lowered" position, using the pitch of the ball-screw actuator, we can calculate how many turns the ball-screw actuator must make to travel between the two points, allowing for precise, repeatable lowering without the need for a distance sensor. Our team identified this method of coarse movement to be a very good option, considering the availability of the ball-screw actuator in Dr. Cullinan's lab, and only varied the methods of fine movement in the following concept generation stage.

4.4 Preliminary Design Concepts

The initial set of preliminary designs were centered on selecting potential fine movement mechanisms, as the coarse movement mechanism was identified as explained in Section 4.2. Other subsystems, such as the frame, while considered, were not the primary focus in this preliminary phase of concept generation.

The first design shown below in Figure 9 centers around the idea of replacing a micrometer knob with a picomotor, a fine resolution linear actuator, to drive a Z-axis stage for fine movement.

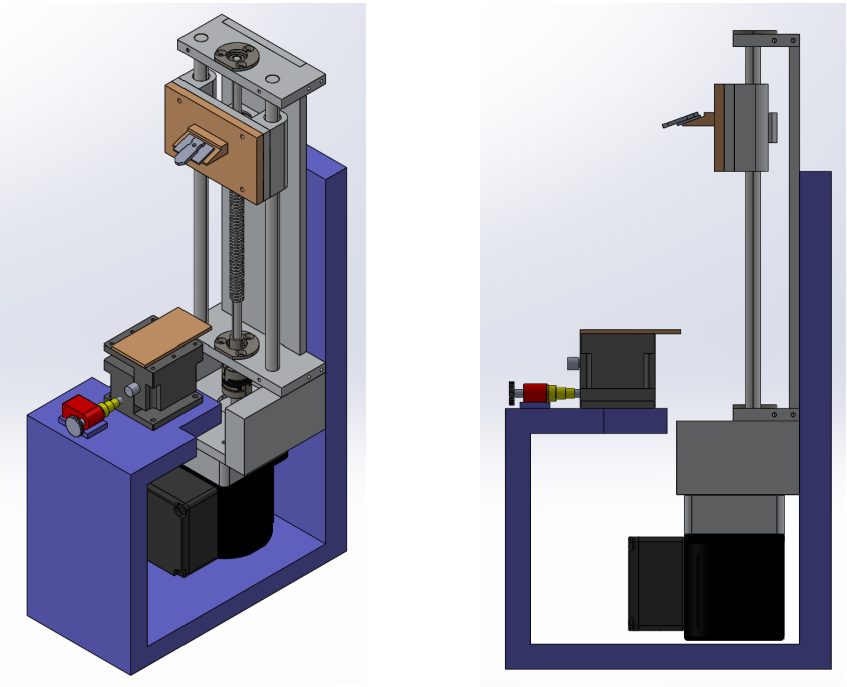

Figure 9. Picomotor Driven Z-Axis Stage for Fine Motion of Sample Stage.

The AFM is attached to the ball screw actuator, which provides coarse movement, and is lowered to about 0.5mm above the sample surface. The picomotor would then drive the micrometer stage up the remaining distance until the AFM tip makes adequate contact with the sample.

A few of the main benefits of this design stem from its simplicity. Since the Z-axis stage and picomotor are off the shelf components, the manufacturing process is simplified since there are fewer components that require machining or assembly. In addition, the Z-axis stage inherently provides smooth vertical motion as it is displaced, which is important during fine motion. After the stage has been displaced, it automatically locks its position, removing the need for an external locking mechanism, which reduces the cost of the device and design complexity. However, although there are videos of motorizing existing translation stages (Thorlabs, 2021), there is no quantitative evidence ensuring that the desired resolution of 0.1μm is achieved. We also cannot be certain that replacing the micrometer knob with a picomotor would not cause damage to the internal hardware of the micrometer. In addition, the picomotor, picomotor driver, and z-axis stage are expensive components, driving up the cost of our design and posing a larger financial risk if the design does not function as expected.

The second generated design shown below in Figure 10 utilizes a picomotor to drive a secondary, smaller ball-screw actuator for fine movement.

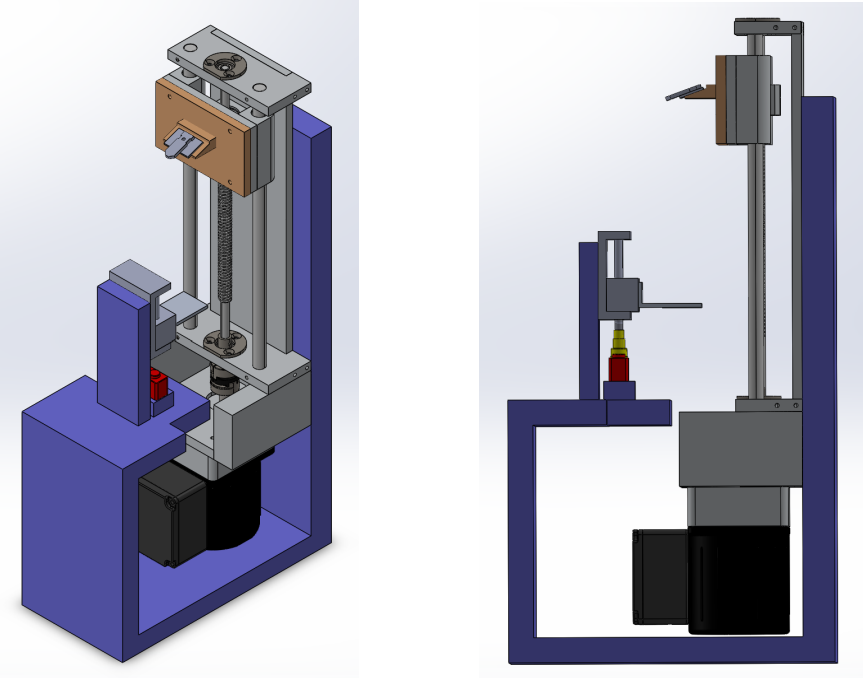

Figure 10. Double Ball Screw Mechanism for Fine Motion of Sample Stage.

Like the first design given in Figure 9, the second design also uses a ball screw actuator for coarse movement. The picomotor would then drive a secondary ball screw to vertically displace the sample stage upward to meet the AFM tip. This design aims to incorporate elements from ICSPI's automated chip lowering mechanism that is advertised along with their benchtop nGauge AFM-on-a-chip, shown in Figure 4 (ICSPI, 2022).

The secondary ball screw actuator, like the first preliminary design, removes the need for a locking mechanism, effectively reducing cost and design complexity. However, manufacturing the secondary ball-screw mechanism would be a complex process. Additionally, due to vibration risks and the inherent friction of a ball-screw actuator, it would be difficult to achieve the necessary fine motion step size resolution of 0.1μm (refer to the Specification Sheet in Section 3).

The last preliminary design shown below in Figure 11 incorporates a linear voice coil driven rail mechanism for fine movement of the sample stage. A voice coil is an essentially frictionless actuator that is made from a winding of metal wire around a permanent magnet. When current is passed through the wire coil, it induces a magnetic field that interacts with the permanent magnet, displacing the coil out of its housing. The distance the voice coil is displaced is directly related to the amount of current passed through the wire coil. A linear voice coil is ideal for precision movement over small distances, which directly matches our application (Industrial Quick Search, n.d.).

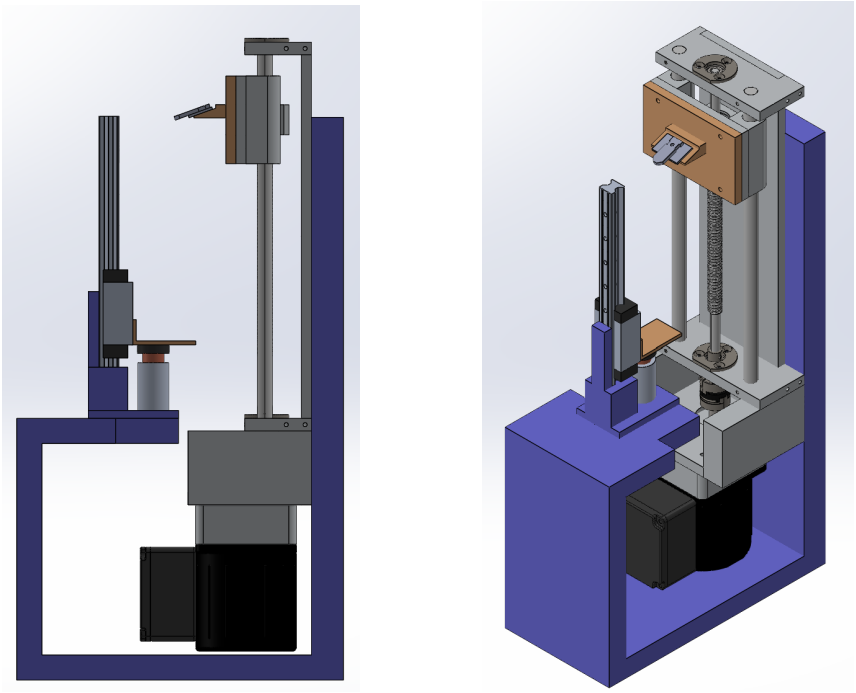

Figure 11. Voice Coil Driven Rail Mechanism for Fine Motion of Sample Stage.

Once again, this design uses a ball-screw actuator for coarse movement. As seen in Figure 11, as current is run through the voice coil, the wire coil is displaced out of its housing, pushing the sample stage upward to meet the AFM tip.

Like the first preliminary design, this design is simple to manufacture and assemble. The guided rail smoothens the instantaneous motion of the voice coil which reduces the risk of the sample stage colliding with the AFM. In addition, the voice coil and rail guided components are cheaper than the components required for the other preliminary designs. However, the rail-guided system re-introduces friction into the system, directly contradicting the benefits of the frictionless voice coil, which affects the resulting resolution of the fine motion.

4.5 Leading Concept Design

After discussing the preliminary designs with Dr. Cullinan and Barbara, we generated a leading concept. The leading concept is a modified version of the voice coil driven rail mechanism design in Figure 11. Rather than using a rail system to guide and smoothen the voice coil movement, a flexure mechanism can be used instead, which is further elaborated upon in Section 4.5 of this report. The leading concept is shown below in Figure 12.

One of the primary goals of the leading concept was for all required components and mechanisms to be easily accessible and to be incorporated into the structure itself (sample stage, AFM circuit boards, motor drivers, amplifiers, DAQs, etc). The voice coil flexure system as shown in Figure 12b is displaced upward a maximum of 0.5mm to meet the AFM that is attached to the machined angled plate that is fixed to the ball-screw actuator. The bottom of the voice coil is fixed to a platform that connects the voice coil and flexure mechanism to the overall device via fasteners, plates, and brackets. The sides of the flexure are fixed via hat brackets screwed into metal side walls. The ball-screw

actuator is positioned at the center of the structure and is supported by a brace to prevent tipping. All possible frame and structure is made from 80/20 T-slot aluminum because of the ease of machining, and the simplicity of fastening all of the components together removably. Additional justification for structure selection will be given in Section 5.

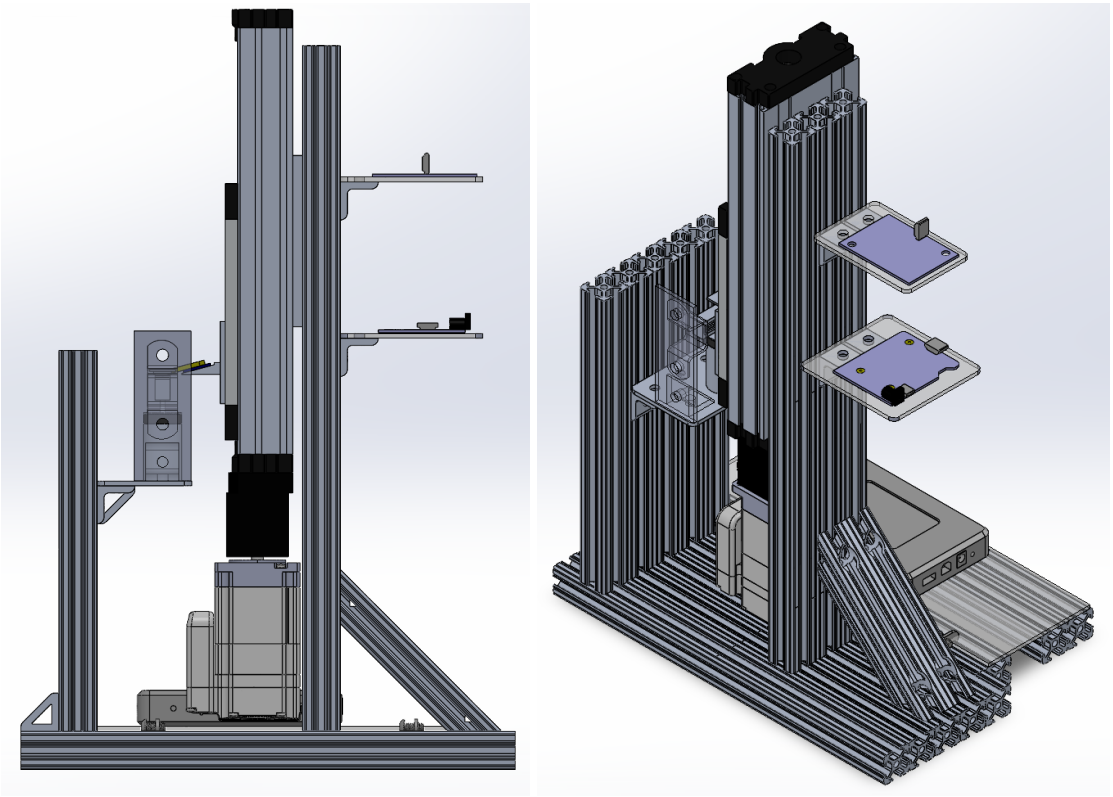

(a)

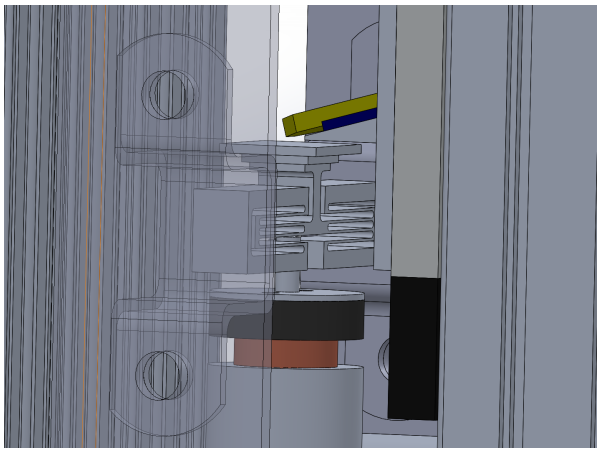

(b)

Figure 12. (a) Overall View of Leading Concept Design using a Voice Coil and Flexure Mechanism, (b) Close Up of Voice Coil and Flexure Mechanism.

On the backside of the ball screw actuator, the required AFM boards are positioned on non-conductive acrylic platforms such that the cable length between the AFM and AFM boards is minimized. Lastly, the microcontroller is located on the outer edge of the structure, placed onto a sheet of acrylic supported by the external 80/20 frame. The structure may be expanded upon in the future depending on the size of our selected power supply and of all ordered components.

4.6 Parallel Double Parallelogram Flexure

In general, a flexure is a frictionless system that acts as a compliance element in a predetermined degree-of-freedom (DOF) when a force is applied to it, while remaining very stiff in all other directions. Flexures also inherently possess deterministic repeatability and have a near infinite lifetime. They are often used in high-precision applications for these reasons. The flexure we are using in our leading design is a parallel double parallelogram flexure. The parallel aspect of the flexure is for increasingly precise movement in only one translational DOF (i.e. the Z-direction), and refers to there being two double parallelogram flexures placed side-by-side (i.e. in parallel) (Smith, Arumugan, & Nijenhuis, 2021). The double parallelogram shape of the flexure is used in fine resolution applications, and, compared to single parallelogram flexures, provides for less kinematic error in the main translational DOF. The two stages of the double parallelogram experience errors, but the errors in the second stage are the reverse of the errors in the first stage, causing the net kinematic error to cancel out (Panas, 2016). Therefore, the resulting effect of the parallel double parallelogram flexure, shown in

Figures 13-15, is to provide for highly precise motion in only the Z-direction with limited kinematic error.

The specific design of the flexure shown in Figure 13 is almost identical to the flexure shown in Yao's 2016 paper, given in Figure 14, but the thicknesses of the beams of the flexure have been modified to give the desired results in the FEA shown in Figure 15.

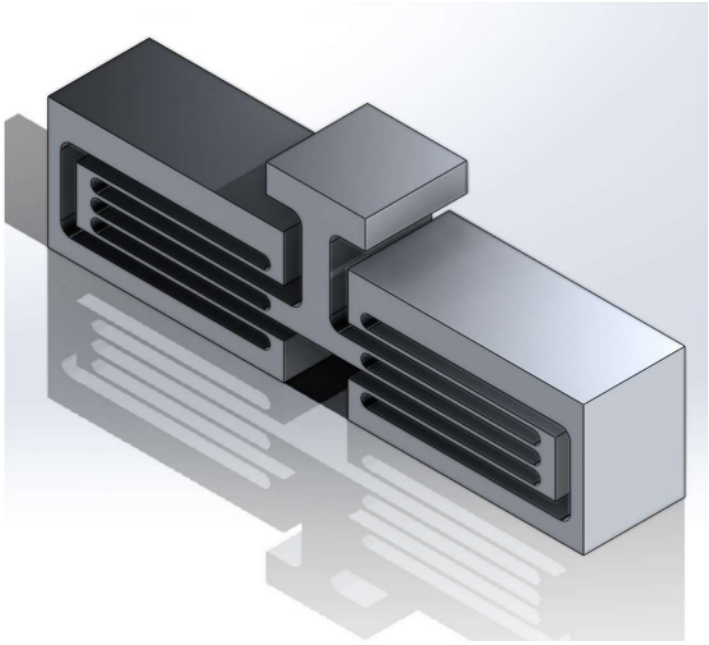

Figure 13. CAD of the Parallel Double Parallelogram Flexure used in the Leading Design.

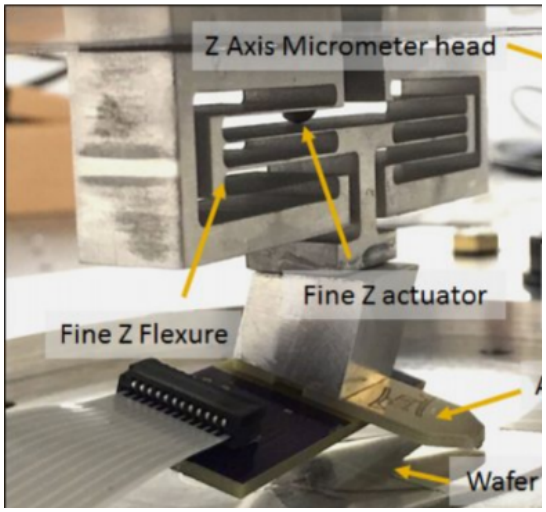

Figure 14. Z Flexure Mechanism. Image from *Yao, et. al.*, by Precision Engineering, Volume 47, 147-157, 2016 (https://doi.org/10.1016/j.precisioneng.2016.07.016).

In addition, an FEA simulation was performed on the flexure shown in Figure 15. The flexure was designed and the beam thicknesses were dimensioned such that the primary translational stage of the flexure (shown as the top of the red "I" beam below) would displace 0.5mm when the voice coil provides 10 N of force. In the FEA, the sides of the flexure were fixed as the sides are also fixed in the leading concept by hat brackets and metal side walls. The force was applied at the bottom of the "I" beam (see pink errors). The results of the FEA simulation are shown below in Figure 15:

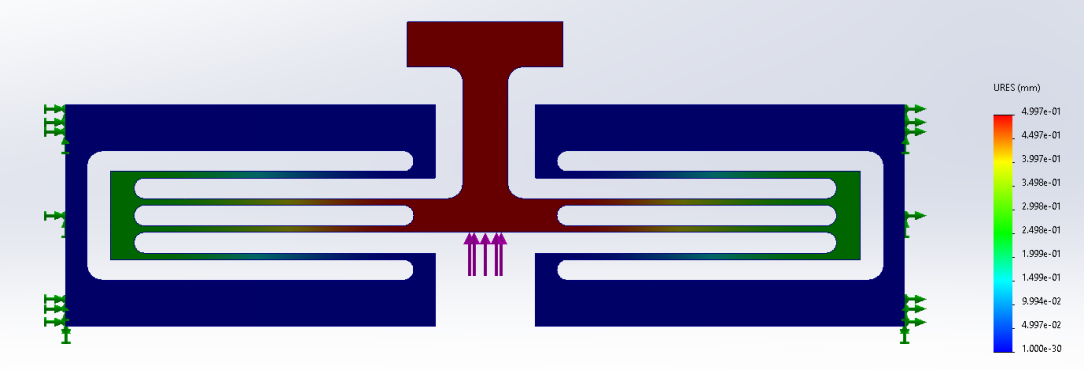

Figure 15. Parallel Double Parallelogram Flexure FEA Simulation.

Analyzing the results, the flexure displaced the desired 0.5mm when 10 N of force were applied, providing confidence in the dimensions of our CAD design.

5 COMPONENT SELECTION

5.1 Ball Screw Actuator

The chosen ball screw actuator is the Parker 404100XR. This specific model has a travel range of 100mm which can provide sufficient clearance for the user to remove and load a sample without touching the AFM After taking physical measurements, the main screw, which drives movement, has a pitch of 5mm, and depending on the selected motor, will provide a desired resolution of 0.1mm. In addition, it has an external limit sensor which may be utilized to control movement.

5.2 Servo Motor and Driver

Before selecting a specific motor model, we identified the ideal type of motor to drive the ball-screw actuator. For this application, we decided that a servo motor would be better than a stepper motor as it can provide smooth continuous motion as the AFM is lowered by the ball-screw actuator, limiting vibration and the risk of damage to the AFM tip.

Other factors to consider were torque output and shaft length. The maximum running torque for the 404100XR ball-screw is 0.11N-m (Parker, 2021, p.15). As for shaft length, the minimal length was found to be about 16mm through physical measurements. The chosen servo motor, the isV57T-090 integrated servo, has a rated torque of 0.3N-m and a shaft length of 33mm (Stepperonline, n.d.). Therefore, the specifications of this motor match well with what is required to operate the ball-screw actuator. In addition, this motor contains a built in driver that possesses a 16-bit encoder, eliminating the need to purchase a separate motor driver to operate our servo. The 16-bit encoder provides sufficiently small counts such that the desired coarse movement resolution of 0.1mm is achieved. The integrated servo

motor we selected is also relatively low cost at less than $100, and would only require a precision 8mm to 8mm linear coupling to connect the servo to the ball-screw actuator for operation.

5.3 Structural Material

The chosen structural material for the frame shown in the leading concept in Figure 12 is 80/20 T-slot aluminum which is made out of 6105-T5 aluminum (McMaster-Carr, n.d.). The main benefit of using 80/20 T-slot aluminum is the ease of positional adjustment. The 80/20 frame will bear the load of the motor and ball-screw actuator, the two heaviest components in our design. These two components, according to their specification sheets, have a mass of 0.98kg and 3kg, respectively, and act as a shear force on the structure. The shear strength of aluminum can be approximated to be 0.65 times its tensile strength. For 6105-T5 aluminum, according to the ASM handbook, the tensile strength is approximately 262 MPa (Anderson, 2019). Making the assumption that the structural beam sustaining the two components is a rectangle whose area is 2in x 6in, the maximum shear stress can be calculated using equation 1 where V is the shear force and A is area.

$$\tau = \frac{3V}{2A} \tag{1}$$

The calculated shear stress was three orders of magnitude less than the shear strength of 6105-T5 aluminum. This means that the structural material is more than sufficiently strong for this use case. 80/20 T-slot is also sufficiently strong to withstand normal handling loads not to exceed 100 lb of force, and is a good choice as the structural frame for our automated tip lowering device.

The plate holding the voice coil, flexure system, and other related hardware as shown in Figure 12 will be made out of 6061-T6 aluminum. According to the ASM Handbook, the strength properties of 6051-T5 are sufficiently similar to 6061-T6, and given that the previous analysis showed that 6051-T5 is sufficiently strong to support the heaviest components of our device, 6061-T6 will likewise be more than strong enough to support the much lighter voice coil and flexure system.

The other plates are made from an acrylic material to speed up the manufacturing process as acrylic does not have to be machined, but rather may be laser cut. Additionally, acrylic is non-conductive, and we can place electrical components on these acrylic platforms without having to insulate them first. As the acrylic plates are only sustaining the load of lightweight circuit boards and electrical components, they will also be sufficiently strong for our application.

5.4 Microcontroller

For our DAQ, we looked into several options and narrowed it down to Arduino UNO and myRIO. We decided to use myRIO for several reasons. First, the myRIO allows us to use Field Programmable Gate Arrays (FPGA) (National Instrument, n.d.). FPGA provides fast and accurate data acquisition (Advance Micro Devices, n.d.**.)**. The Arduino can run at a clock rate of 16MHz (ElectroSoftCloued, June 2020) and the myRIO can run at 40MHz (National Instrument, n.d.). Given the accuracy needed for our control system, the clock rate of the myRIO is crucial to not overshoot our movement and destroy the AFM chip. Additionally, the myRIO has multithreading (National Instruments, August 2022), which allows us to run multiple programs at once. This is a

necessity, since we will be controlling multiple actuators and each has its control system. Arduino does not support multithreading. myRIO also has a better processor with a processing speed of 667MHz (National Instrument, n.d.) compared to 16MHz (ChipWired, n.d.) in the Arduino UNO. Since we decided to use the myRIO, we decided to use LabVIEW to maximize the myRIO's capabilities.

5.5 Voice Coil

The selection of the LVCM-025-038-01 Linear Voice Coil Motor Actuator was informed by Yao, 2016, which also used this brand of voice coil in conjunction with a parallel double parallelogram flexure system. Figure 16 below shows how the force output of the voice coil changes with the stroke of the actuator. This graph shows that the voice coil can output a force of more than 10N at a stroke of around 0.150 inches (Moticont, n.d.). For the purposes of our flexure system FEA shown in Section 4, Figure 15, we used a maximum force of 10N, which is quantitatively achievable using this voice coil, to inform our displacement of 0.5mm.

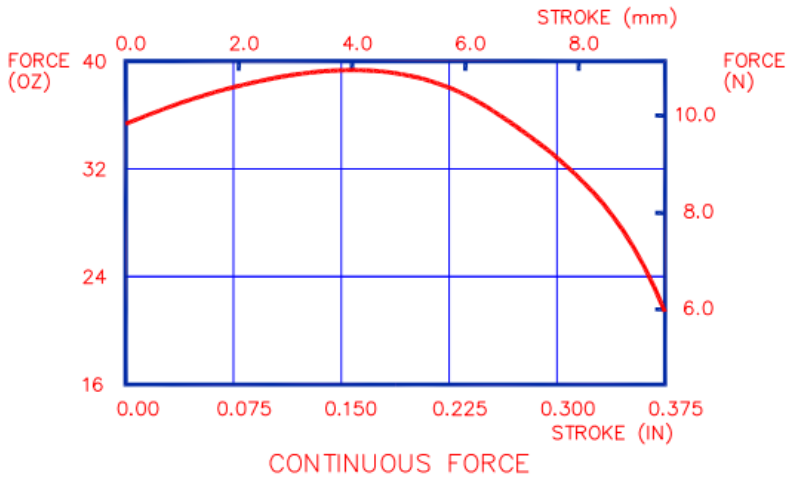

Figure 16. Force vs Stroke Data for the LVCM-025-038-01 Linear Voice Coil Motor Actuator. Image from Monticont, n.d., (https://www.moticont.com/lvcm-025-038-01.htm).

6 BILL OF MATERIALS

Table 2 below presents the bill of materials, current as of March 20th. The bolded items in the table represent items that our team and sponsor are purchasing. The asterisked items are what is currently available to us at no personal cost through Dr. Michael Cullinan's lab. Additionally, the '~' represents a rough cost estimate of the listed item. Selection of the majority of the listed components, excluding hardware choices, is elaborated upon in Section 5 of this report.

Our group hopes to have our flexure system commissioned to be cut by either waterjetting or wire EDM, and based on preliminary quotes, it may cost as much as $200 to have our flexure precision manufactured. Unfortunately, the capabilities of the waterjet cutters on the University of Texas campus are not adequate for the purpose of machining this flexure system.

Another item to mention is the 100W Audio Power Amplifier Module Board. This will be used to amplify the signal from the AFM chip to the voice coil during the closed-loop feedback control of fine movement, which is further elaborated on in Section 8. While Barbara and Dr. Cullinan currently have one of these boards, an additional one may need to be used to amplify the signal between the myRIO and the motor driver. In the case that a second board will need to be used, an additional purchasing cost of $41.31 will be added to the total price listed in Table 2 below. It should be noted that the listed prices do not include any processing fees or shipping and handling costs, but even with these additional costs, our device will be sufficiently under budget.

Table 2. Bill of Materials

Item	Supplier/Part #	Quantity	Listed Net Price [$]
80/20 T-slot Al*	McMaster Carr	-	-
80/20 T-slot L Bracket*	McMaster Carr	17	-
Ball-Screw Actuator*	Parker 404XR Series [404100XR]	1	-
Voice Coil*	MotiCont LVCM-025-038-01	1	-
myRIO-1900*	National Instruments	1	-
DC Power Supply*	BK Precision 1744A	1	-
100W Audio Power Amplifier Module Board*	EC Buying - Sold by Ebay [OPA549]	1	$41.31
0.25” 6061-T6 Al*	McMaster Carr	12” x 12”	-
Double-sided Tape*	-	As needed for insulating layers	-
MechBlocks*	Motus Mechanical M-S-012	1	-
Distance Sensor*	Baumer OADM 13164/405869	1	-
Hardware*	Assorted lengths and sizes of M6, M5, M4 fasteners-	As necessary	-
80/20 T-nut Assemblies*	McMaster Carr	33	-
10mm 7075-T6 Al Flexure System	**Commissioned - TBD**	**1**	**~200 or as quoted**
80/20 T-nut Hardware	**McMaster-Carr**	**6**	**18.30**
80/20 T-slot Double Gusset	**McMaster-Carr**	**3**	**45.60**
Integrated Servo Motor	**StepperOnline [isV57T-090]**	**1**	**92.75**
8-8mm 7075 Al Clamping Precision Flexible Shaft Coupling	**McMaster Carr**	**1**	**67.13**
304 Stainless Steel U-Shaped Connector Bracket	**Uxcell - Sold by Amazon**	**1**	**12.99**
⅛” Acrylic (24” x 24”)	**Texas Inventionworks**	**1**	**10**
¼” Acrylic (24” x 24”)	**Texas Inventionworks**	**1**	**10**
			~456.77

7 FINAL DESIGN AND PROTOTYPE

7.1 MechBlocks Flexure

The designed flexure discussed in Section 4.6 was unable to be machined using resources available at the University of Texas at Austin due to non-functionality of the water-jet cutter and unavailability of the wire EDM machines. Our sponsor looked elsewhere to commission the flexure, however, commissioning was either too expensive (on the magnitude of ~$200-$300) or there were significant concerns about lead times within the shipping process. As such, our sponsor recommended using Motus Mechanical's M-S-012 MechBlocks, which is a toolkit of blocks, leaf springs, and assorted hardware that can be used to construct a temporary flexure mechanism (Motus Mechanical, n.d.). The MechBlocks flexure we designed is shown below in Figure 17.

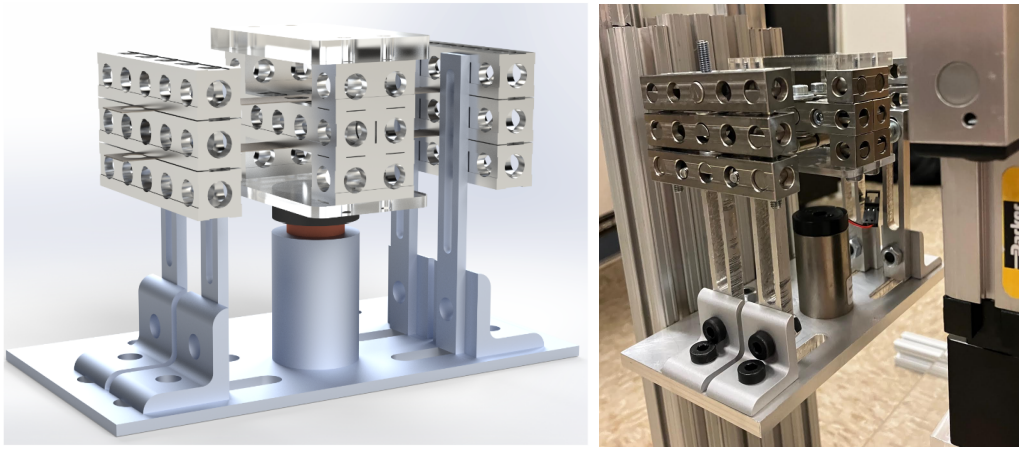

Figure 17. Mechblocks Flexure CAD Model and Prototype.

The constructed MechBlocks flexure is a parallel double parallel flexure mechanism, functionally similar to that of the originally designed flexure in Figure 13. The stiffness of the system is determined by the horizontal position at which the flexure leaf springs–thin sheets of flexible steel–are fixed. To determine the position to achieve a

0.5mm displacement with 10N of force, an FEA study was conducted and is shown in Figure 18.

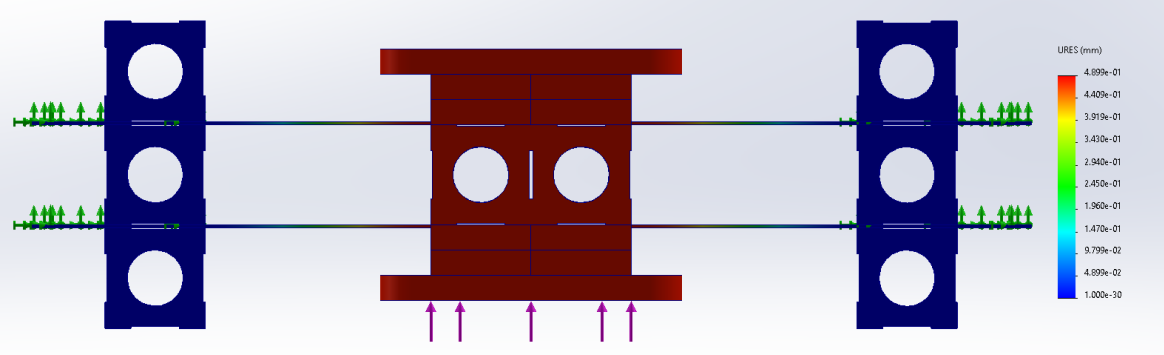

Figure 18. MechBlocks Flexure FEA.

From the study, the approximate fixed position was determined to be about 0.87 inches from the outer edge of the flexure spring. Referring to the structure shown in Figure 17, it can be seen that we designed the bottom plate to enable shortening or lengthening of the leaf springs with relative ease, allowing for the L-brackets connecting the slotted flexure side walls to be fastened at any point along the slots in the bottom plate. Furthermore, we ensured that the flexure itself could be raised or lowered relative to the voice coil by implementing four (4) slotted side walls with associated fastener and washer systems.

After further discussion with our sponsor, it was decided that they would machine the original flexure shown in Figure 13 after the project's completion and replace the MechBlocks flexure with it. To enable the swapping of the flexures, we designed the following structure shown below in Figure 19.

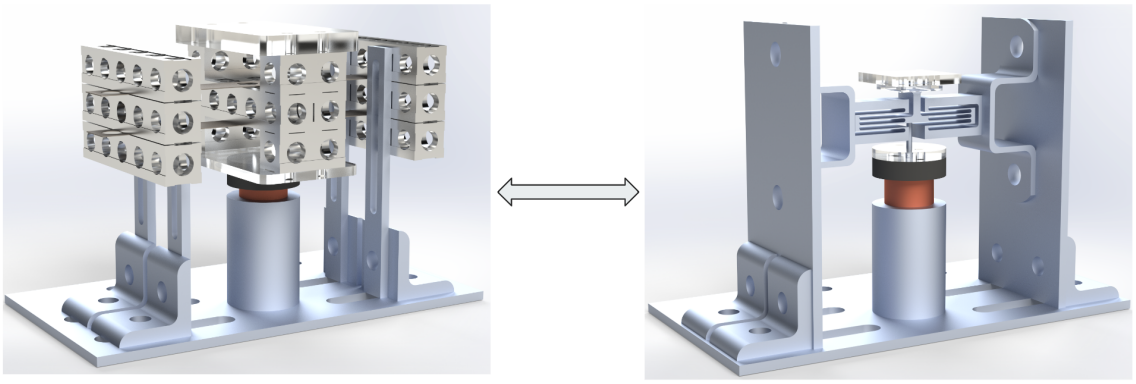

Figure 19. Swappable Flexure Design.

To replace, the user would simply remove the vertical slotted side walls and MechBlocks flexure and replace them with the plates and brackets that sustain the machined flexure. It should be noted that new acrylic plates may need to be laser cut to fit the new flexure system.

7.2 Laser Distance Sensor

Initially, as outlined in Section 4.3, we removed the need for a distance sensor as our team determined the variability in sample thickness would be negligible. As explained, this would allow us to lower the ball-screw actuator by a repeatable distance, effectively lowering the AFM probe to about 0.5mm above the sample surface without a distance sensor. However, after further discussion with our sponsor, she concluded that the sample thickness can vary by a significant amount and deterministic repeatability in our coarse motion stage may not be sufficient. To take into account varying sample thickness, we decided to incorporate a laser distance sensor into our mechanism which would function in conjunction with the ball-screw actuator.

The specific sensor we implemented into our prototype is the Baumer OADM 13164/405869 laser distance sensor. The laser possesses a 2mm diameter laser and a resolution of 0.01mm which is sufficient for our application since the samples themselves will be 0.25in x 0.25in and the AFM needs to be lowered to 0.5mm above the sample surface (Baumer Electric, n.d). Fortunately, we were able to machine a mount for this laser distance sensor easily, by adding two (2) holes to the back plate holding the machined angle piece for the AFM chip, and adding a small adjacent plate equipped to mount the distance sensor, shown in Figure 20. This mount enables the laser distance sensor to lie about 60mm above the AFM chip.

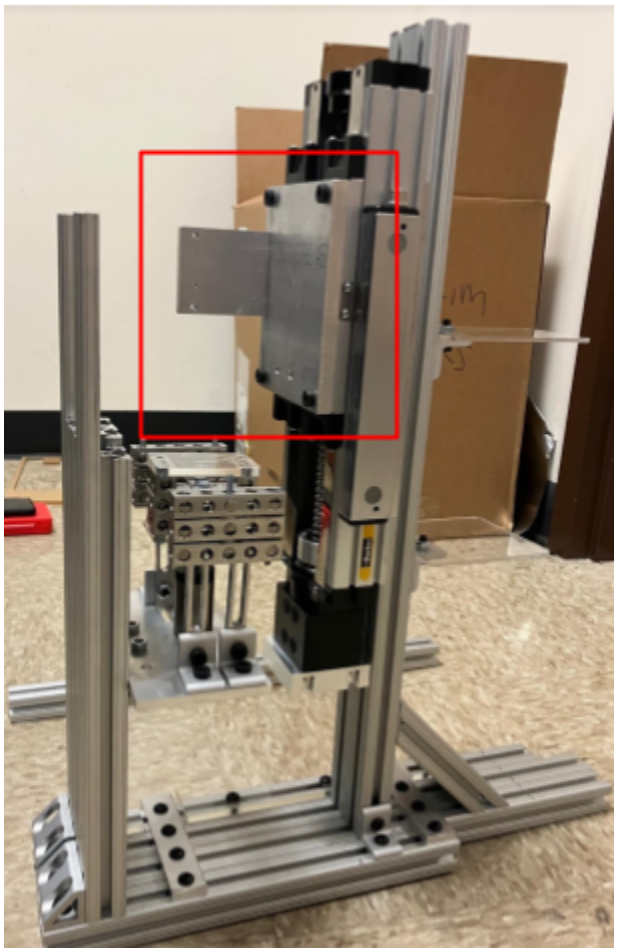

Figure 20. Machined and Assembled Laser Distance Sensor Mount.

7.3 Final Prototype Hardware

Referring to Figure 21, the final CAD of our prototype hardware to be delivered ended up being similar to the leading concept discussed in Section 4.5 with the exception of the flexure system and the addition of the laser distance sensor. The final design necessitates the machining of a slotted flexure system and voice coil base, four (4) slotted side walls for the flexure, the building of the MechBlocks temporary flexure, laser cutting of two (2) acrylic stages (one for the voice coil to push on and one to hold the sample), and the machining and assembly of the laser distance sensor mount and hardware.

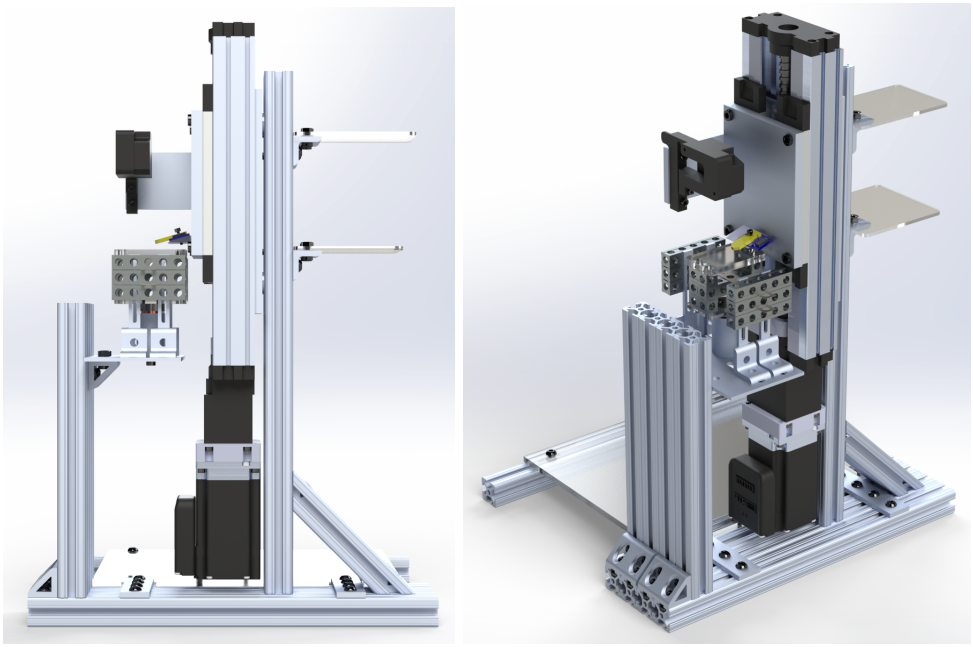

Figure 21. Final Computer Aided Design of Automated AFM Tip Lowering Mechanism.

After machining and purchasing of all necessary hardware, we were able to assemble the final prototype hardware, shown in Figure 23. 80/20 T-slot aluminum was machined to size and assembled as shown in Figure 21 using associated 80/20 hardware,

including double gussets, L-brackets, angle brackets, and two (2) connector plates our team machined ourselves. An acrylic platform used to hold any necessary electrical components, such as the MyRIO, was affixed to the aluminum structure. The ball-screw actuator was suspended on a connector plate connected to the 80/20 structure, and another connector plate was fastened to the front of the ball-screw actuator to hold the machined 15° aluminum piece for the AFM chip and the laser distance sensor mount. Hardware assembly instructions are given in Appendix C.

The most difficult manual machining our team encountered was the fabrication of the angled AFM chip holder, shown in Figure 22. The figure below shows the third iteration of this piece. The tight tolerances, small holes, and necessity of a thin piece with a 15° slant resulted in two scrapped pieces due to compressed threads and incorrect hole dimensions, respectively. In the end, the final, correct iteration was created by piloting holes directly through a scrap AFM circuit board, shown in Figure 22, to eliminate dimensional error.

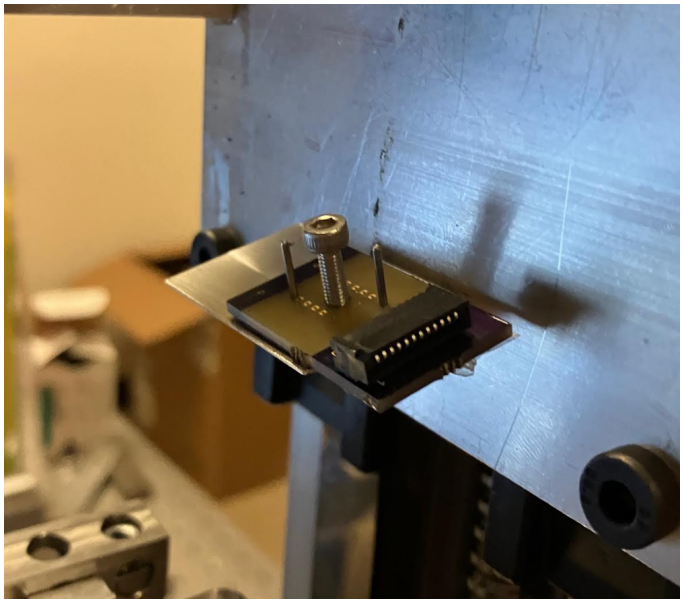

Figure 22. Machined Angled Piece to Hold the AFM Chip and Associated Circuit Board.

The slotted flexure system and voice coil base plate was suspended on the 80/20 with two angle brackets, and the voice coil was screwed into the center hole in this plate. The flexure system was assembled and fixed onto the four (4) vertical slotted side walls at the appropriate width and height via 80/20 L brackets and necessary hardware. A ⅛" thick acrylic stage was fastened to the bottom of the flexure and another ¼" thick acrylic sample stage was slid onto the exposed ends of the flexure fasteners, firmly holding the stage onto the flexure. The servo motor was connected to the ball-screw actuator via a machined motor mount and 8-8mm flexible shaft coupling. Finally, acrylic stages to hold the remaining two (2) AFM circuit boards were affixed to the back of the 80/20 structure at the appropriate height to wire all components together without strain on the electrical components, namely the electrical wiring. The entire structure was fastened down to the optical table using 80/20 L-brackets. Several photos of our final prototype are given in Appendix B of this report.

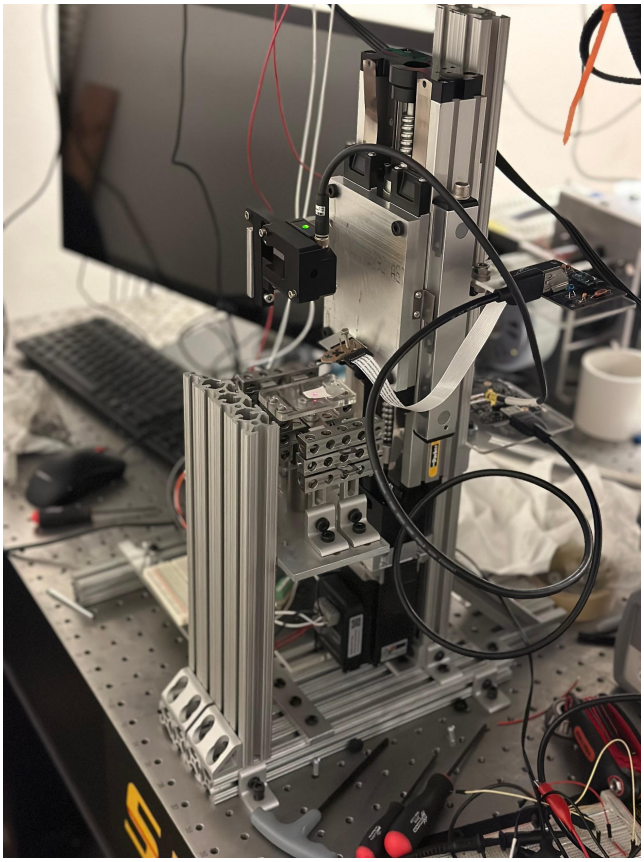

Figure 23. Final Assembly of Prototype Hardware.

7.4 Vibration Analysis

As mentioned throughout the report, vibrations must be minimized to ensure accurate AFM scans. To examine the effects of vibration on our assembled system, we conducted frequency FEA studies in SolidWorks. The effects of vibration were tested for the device with both Mechblocks flexure and the flexure outlined in Section 4.6. Both studies were necessary due to the eventual replacement of the MechBlocks with the water-jetted or wire EDMed flexure system. Figure 24 below highlights via the green arrows shows how the structure is fixed along the bottom for the FEA studies. Table 3 below summarizes the FEA results for both flexures.

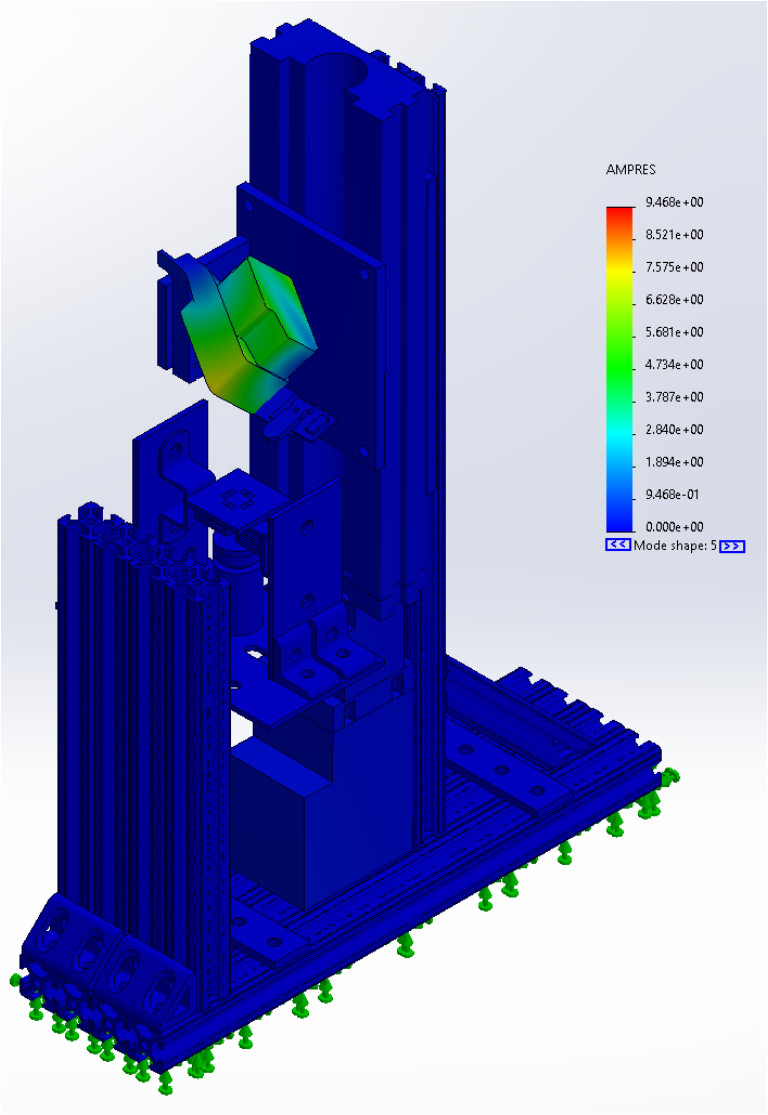

Figure 24. FEA Vibration Study for Machined Flexure in Mode 5.

Table 3. Frequency FEA Results for Structure

Flexure	Mode 1 Frequency (Hz)	Mode 2 Frequency (Hz)	Mode 3 Frequency (Hz)	Mode 4 Frequency (Hz)	Mode 5 Frequency (Hz)
MechBlocks	31.318	49.041	58.859	67.318	94.684
Machined	31.262	49.115	59.619	67.158	123.98

The system itself will lie on an optical table, which dampens frequencies over around 30 Hz. Analyzing table 3, all modal frequencies were found to be above 30 Hz. In addition, swapping the type of flexure from MechBlocks to machined only affected the modal frequency of mode 5, which were both over 90 Hz. As the optical table can dampen frequencies over 30 Hz, these results imply that the optical table will dampen any frequencies that may affect the structural integrity of the system. Further vibrational analysis comparing in-plane to out-of-plane vibrational deformations was not considered due to the results proving the dampening capability of the optical table for our specific structure.

8 SOFTWARE/CONTROL SYSTEM

8.1 Program Overview

For our control system, we decided to use a four (4) event structure for our code. When initialized, it turns the servo motor on and moves the AFM chip to the top of the ball-screw actuator, which has a physical limit. It will then use the servo motor to lower the AFM chip to 0.5mm from the sample stage. The voice coil will then move the stage closer to the AFM until the AFM chip is at an adequate distance from the sample. The piezoresistor in the AFM chip is used to inform the fine motion until the optimal distance between the sample and the AFM chip is achieved.

A user interface (UI), shown in Figure 25, was constructed to allow the user to input setpoints, proportional-integral-derivative (PID) controller coefficients, and other necessary parameters into the system. The four (4) event structure is initiated by pressing the ‘Initialize’ button for the servo motor, beginning the coarse movement until the set point is achieved, informed by the distance sensor feedback. Once this stage of motion is complete, the ‘CoarseMovementDone’ indicator will turn green. At this point, the ‘Voice Coil Control’ may be switched ‘on,’ beginning the fine motion phase. At the point that the AFM probe makes adequate contact with the specimen as indicated by the AFM piezoresistive sensor, the ‘FineMovementDone’ indicator will turn green and all motion will cease for scanning. Throughout both stages of movement, motion can be monitored using the amplitude v. time position and velocity graphs shown to the right of the UI. At any point that unexpected motion is detected by the user, the ‘STOP’ button may be pressed to abort the motion operation.

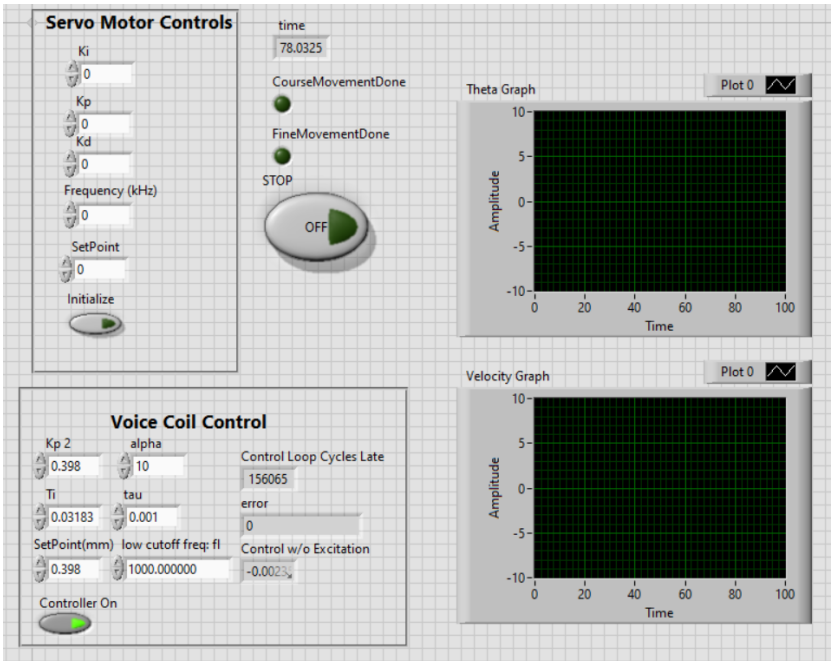

Figure 25. User Interface for the Two Stages of Motion.

8.2 Coarse Movement

Our device's coarse movement will use a closed-loop control mechanism, programmed via LabVIEW and MyRIO to control the motion of the AFM chip. The servo motor will move the ball-screw actuator to bring the AFM tip to 0.5mm of the sample stage at the beginning of every scan. While the motion will not have to be as precise as the fine motion, the coarse motion should be precise and consistent enough to bring the AFM tip accurately to a distance of 0.5mm from the sample surface without unexpected collisions between the AFM probe and the sample. A user input setpoint in the form of a distance between the AFM chip and the sample is necessary. This setpoint is input into the program via the UI shown in Figure 25. The virtual 'Initialize' button for the servo motor must be clicked to initiate motion. The LabVIEW code then uses the setpoint and feeds it into a comparator, which converts the distance into a velocity. The

output velocity is then fed into a PID controller and a speed controller. Lastly, the speed controller outputs, through the MyRIO-1900, a pulse width modulation (PWM) to control the motor. For our feedback mechanism, we are using a laser distance sensor with a resolution of 0.01mm (see Section 7.2). To reduce the noise from the laser sensor, we used a Bessel 2nd order lowpass filter, with a cutoff frequency of 1kHz. After the scan is complete, the servo motor will reverse its motion and reposition the AFM chip back to the home position, ready for the next scan. This coarse motion code can be seen in Appendix D of this document. An electrical wiring diagram for this system can be found in Appendix E.

8.3 Coarse Motion Trials

Our team attempted coarse motion trials using a broken AFM chip and completed coarse motion code, but saw some unpredictable behavior from our coarse motion system. Inputting PID coefficients of $K_I = 0$, $K_p = 0.25$, and $K_d = 0.03$ into the UI, we saw a reasonably small amount of overshoot from our coarse motion system–on the order of 0.1mm–, but we did still see unignorable instability in the system. Settling time was extremely long and the consistent oscillation around the set point proved to be an issue with our system hardware. When removing power from the servo motor, rendering the ball-screw actuator motionless, we still saw this level of distance measurement oscillation, evidencing that the laser distance sensor itself is the cause of this error. The PID controller for the distance sensor itself must be revisited to enable a more controlled, stable system. Our team is confident that with PID controller tuning for the servo motor, our product is a feasible solution for coarse motion lowering of the AFM tip. The system

showed no concerning vibration, was easy to shut off in the event of unexpected motion, and could lower from 20mm to 5mm, nominally, in less than three (3) minutes.

In future work on this prototype, our team would suggest running the coarse motion trials as we had originally planned. Five separate trials should be run, lowering the AFM from the 'home' position to 0.5mm above the sample surface. Time to lower should be measured and recorded for each trial, overshoot of the distance should be monitored, and, after settled, true distance between the AFM probe and the sample surface should be measured to verify the accuracy of the system.

8.4 Fine Movement

For our fine movement, we decided to implement a closed-loop control system. We took inspiration from the voice coil control in Yao, 2016, which can be seen in Figure 26. We created a while condition to run the closed-loop control system of the voice coil while the ball-screw actuator lowers the AFM chip to 0.5mm from the sample stage and the AFM is therefore not touching the sample. For the feedback control, we decided to use the piezoresistor in the AFM chip. The piezoresistor in the AFM measures the magnitude of the free oscillation of the AFM cantilever. When the AFM approaches the sample, the magnitude of the oscillation will decrease as it is hitting the sample's surface. It will then signal to the software it has reached the stage.

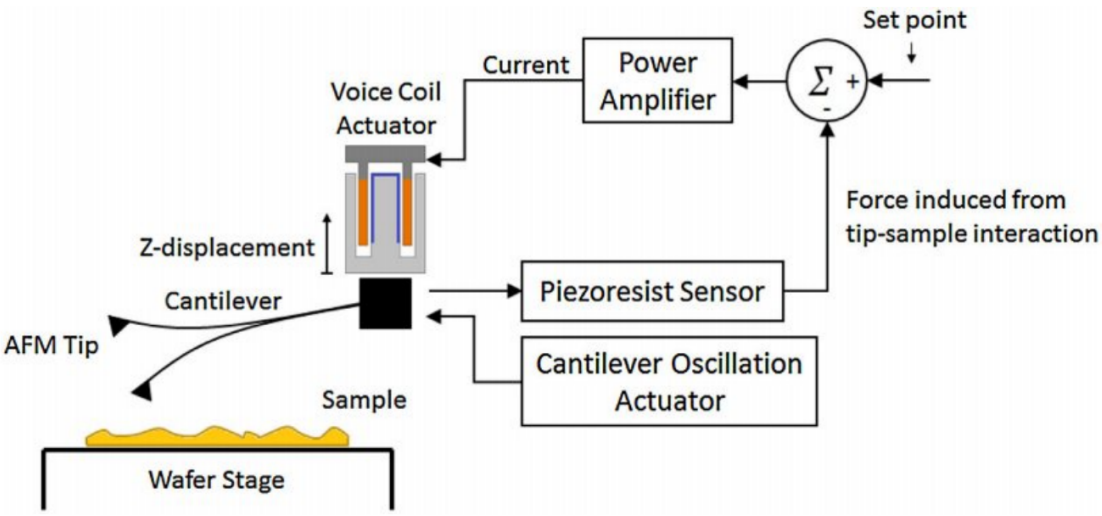

Figure 26. Closed-loop Control System of Voice Coil Actuator. Image from *Yao, et. al.*, by Precision Engineering, 2016.

Unfortunately, as our team began this project with no LabVIEW familiarity, the unforeseen obstacle of learning a new programming language hindered our ability to complete all of the code to make this prototype fully functional. The slightly modified base code we were given can also be seen in Appendix D.

8.5 PID Coefficient Analysis

As mentioned previously, the prototype is designed such that a new machined flexure can be swapped in for the current MechBlocks flexure. Although the MechBlocks flexure and machined flexure will possess similar stiffness values, they will not be identical. Due to the difference in stiffness, the corresponding PID coefficients K_p,Kk_i, and K_d for the fine movement control system must be updated for the machined flexure. Rather than determining these coefficients through experimentation, we constructed a MATLAB program that automatically calculates a set of optimal coefficient values based

on the properties of the flexure (University of Michigan, n.d.). The PID controller we created is shown in Appendix F, using the parameters of the MechBlocks flexure to output PID coefficients and simulated plant+controller behavior.

By modeling the flexure as a forced mass spring damper system, we determined the transfer function for the system as $\frac{1}{ms^2+bs+k}$. Utilizing MATLAB's Control System Toolbox and the established transfer function, we were successful in automatically finding optimal PID coefficients for a given parallel double parallel flexure. It should be noted that the code requires three (3) user inputs for m, k, and b. Mass, m, and system stiffness, k, can be fairly accurately determined using the SolidWorks CAD functionality. The damping coefficient, b, will be more difficult to determine. The flexure system will at least be lightly damped (b = 0.01), but damping below a b of 0.01 is also possible (Thomas, n.d.). A system ID must be conducted for both flexure systems to correctly determine the correct b in order to avoid a guess and check method of determination. Unfortunately, these system IDs were outside the boundaries of our capabilities, but upon determination of the correct b value for the system, our PID tuner should be a useful tool in quickly determining the PID coefficients for recalibration of the fine motion code.

9 CONCLUSIONS AND REMAINING WORK

At the conclusion of this report, a final prototype has been machined and assembled. Instructions for reassembly of this prototype are provided in Appendix C. With foresight into the replacement of the MechBlocks flexure with a machined flexure, the prototype has been designed and machined to allow for easy replacement of these components. All CAD for the delivered prototype and for the necessary components for the machined flexure system are delivered to the sponsor as part of the final deliverable package.

With regards to the software, the coarse motion for the servo motor and ball-screw actuator has been completed in LabVIEW with MyRIO-1900 compatibility. This code incorporates the use of the Baumer laser distance sensor discussed in Section 7 of this report. Preliminary trials of this code have been done using the assembled prototype to promising success. Code has also been written to allow communication between the coarse and fine motion in between the two steps, although trials have not been run verifying its efficacy due to the incompleteness of the fine motion code.

Base code for the fine motion portion of the AFM lowering is written, but due to obstacles encountered in the learning and implementation of LabVIEW, is not fully functional. Communication within the AFM chip's piezoresistive sensor must be established within the code to allow for adequate lowering, and trials must be conducted to verify the code's accuracy. Our team estimates an absolute minimum of 2 hours of remaining work on this fine motion code, given the code writer is very familiar with LabVIEW. To assist in inputting the appropriate parameters into the fine motion code, our team has created a PID tuner that will output the appropriate PID coefficients given user

inputs of m, b, and k for the system. All code and programs will be provided to the sponsor in the assembled deliverables package.

References

[1] Advance Micro Devices. (n.d.). *What is an FPGA?*. Retrieved March 19, 2023, from https://www.xilinx.com/products/silicon-devices/fpga/what-is-an-fpga.html#:~:text=Field%20Programmable%20Gate%20Arrays%20(FPGAs,or%20functionality%20requirements%20after%20manufacturing

[2] AFM setup. Toyosaki, T. (2015, April 22). *Typical Configuration of an AFM*. Retrieved from https://en.wikipedia.org/wiki/Atomic_force_microscopy

[3] Anderson, K., et al. (2019). Properties and Selection of Aluminum Alloys. *ASM Handbook.* Volume 2B, 376-377. https://doi.org/10.31399/asm.hb.v02b.9781627082105

[4] Baumer Electric. (n.d). *Distanz-Sensor OADM 13I64/405869.* [Product Data Sheet].

[5] Bullen, H., & Wilson, R. (October, 2022). *Atomic Force Microscopy.* https://chem.libretexts.org/Bookshelves/Analytical_Chemistry/Supplemental_Modules_(Analytical_Chemistry)/Microscopy/Scanning_Probe_Microscopy/03_Basic_Theory/02_Atomic_Force_Microscopy_(AFM)

[6] ChipWired. (n.d.). *How Fast is an Arduino: Guide to Arduino Speeds.* Retrieved March 19, 2023, from https://chipwired.com/arduino-speed-guide/

[7] ElectroSoftCloud. (June 14, 2020). *Changing the Arduino Clock Speed*.Retrieved March 19, 2023, from https://www.electrosoftcloud.com/en/changing-the-arduino-clock-speed/

[8] Etzler, F., et al. (2012). *Atomic Force Microscopy for Characterization of Surfaces, Particles, and their Interactions.* Developments in Surface Contamination and Cleaning. (307-331). https://doi.org/10.1016/B978-1-4377-7883-0.00006-7

[9] Industrial Quick Search. (n.d.). *Voice Coils*. Types, Materials, Applications, and Benefits. Retrieved March 19, 2023, from https://www.iqsdirectory.com/articles/electric-coil/voice-coils.html

[10] McMaster-Carr. (n.d.). *T-Slotted Framing.* https://www.mcmaster.com/47065T101/

[11] Moticont. (n.d.). *Linear Voice Coil motor actuator LVCM-025-038-01, Continuous Force: 2.5 lb (11.0 N), stroke: 0.37 in (9.5 mm)*. Retrieved March 19, 2023, from https://www.moticont.com/lvcm-025-038-01.htm

[12] Motus Mechanical. (n.d.). *Motus Mechanical*. Motus Mechanical Kits. Retrieved April 18, 2023, from https://www.motusmechanical.com/products/kits

[13] National Instruments. (Aug. 26, 2022). *Multithreading in LabVIEW Real-Time.* Retrieved March 19, 2023, from https://www.ni.com/en-us/support/documentation/supplemental/15/multithreading-in-labview-real-time.html

[14] National Instruments. (n.d.). *myRIO-1900 Getting Started Guide and Specifications*. Retrieved March 19, 2023, from https://www.ni.com/docs/en-US/bundle/myrio-1900-getting-started/resource/376047d.pdf

[15] NANOSCALE DESIGN MANUFACTURING LABORATORY. (n.d.). *Barbara Groh*. Retrieved from http://ndml.me.utexas.edu/members/barbara-groh

[16] NANOSCALE DESIGN MANUFACTURING LABORATORY. (n.d.). *Dr. Michael Cullinan*. Retrieved from http://ndml.me.utexas.edu/members/dr-michael-cullinan

[17] *Ngauge AFM*. ICSPI. (2022, November 2). Retrieved January 29, 2023, from https://www.icspicorp.com/ngauge/

[18] Olin, H., et al. (2003). *Micropositioning device.* (European Patent No. EP1340112A1). European Patent Office. https://worldwide.espacenet.com/patent/search/family/020282086/publication/EP1340112B1?q=pn%3DEP1340112A1

[19] Otto, K.N, & Wood K. (2001). Product Design: Techniques in Reverse Engineering and New Product Development. Upper Saddle River, NJ: Prentice Hall.

[20] Pan, S-P., et al. (2005). *Long-stroke, high resolution nanopositioning system.* (U.S. Patent No. 7307370B2). U.S. Patent Office. https://image-ppubs.uspto.gov/dirsearch-public/print/downloadPdf/7307370

[21] Panas, R. M. (2016, June 23). *Large displacement behavior of double parallelogram flexure mechanisms with Underconstraint Eliminators*. Precision Engineering. Retrieved March 19, 2023, from https://www.sciencedirect.com/science/article/abs/pii/S0141635916300885

[22] Parker. (2021). *404/406XR Series Product Manual.* https://www.parker.com/content/dam/Parker-com/Literature/Electronic-Motion-Controls/Product-Manuals/404XR-406XR-Manual-100-5320.pdf

[23] Shu, D., Lai, B., Kearney, S. P., Anton, J. W., Liu, W., Maser, J. M., Roehrig, C., & Tischler, J. Z. (2020, May 26). Method and Precision Nanopositioning Apparatus with Compact Vertical and Horizontal Linear Nanopositioning Flexure Stages for Implementing Enhanced Nanopositioning Performance.

[24] Smith, S., Arumugam, K., & Nijenhuis, M. (Nov. 2, 2021). *Evaluation of Flexure Mechanism Motion Constraints During Design (Part I and II).* [PowerPoint presentation]. ASPE Annual Conference, Minneapolis, Minnesota, USA. https://aspe.net/tutorial-tutors/36-smith/

[25] Stepperonline. (n.d.). *Nema 23 Integrated Easy Servo Motor 90w 3000rpm 0.3Nm(42.49oz.in) 20-50VDC Brushless DC Servo Motor.* https://www.omc-stepperonline.com/nema-23-integrated-easy-servo-motor-90w-3000rpm-0-3nm-42-49oz-in-20-50vdc-brushless-dc-servo-motor-isv57t-090

[26] Thomas, M. (n.d.). *Flexures*. Retrieved April 18, 2023, from https://web.mit.edu/mact/www/Blog/Flexures/FlexureIndex.html

[27] Thorlabs. (2021). *How to Motorize a Manual Translation Stage | Thorlabs Insights* [Video]. YouTube. https://www.youtube.com/watch?v=hYR27A8mfUs

[28] University of Michigan. (n.d.). Introduction: PID Controller Design. Control Tutorials for MATLAB and Simulink - Introduction: PID Controller Design. Retrieved April 18, 2023, from https://ctms.engin.umich.edu/CTMS/index.php?example=Introduction§ion=ControlPID

[29] Yao, T., Duenner, A., & Cullinan, M. (2016). In-line metrology of nanoscale features in semiconductor manufacturing systems. *Precision Engineering,* Volume 47, 147-157. https://doi.org/10.1016/j.precisioneng.2016.07.016

APPENDIX A: **GANTT CHART**

The Gantt Chart included in this appendix is a living document that is intended to be referenced and updated throughout the entire semester-long project. Due to the size of the Gantt Chart, which has been constructed on Google Sheets, it is split into the three separate images below. It is updated as of the date of this document, April 19, 2023.

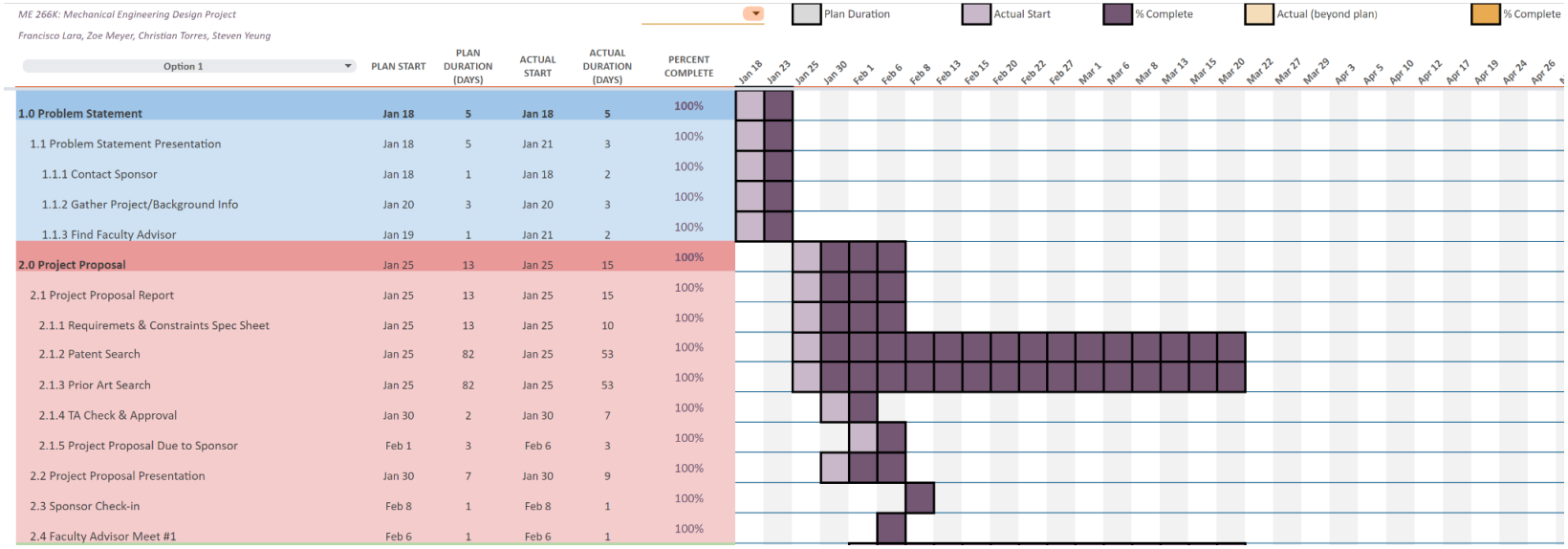

Figure A.1. Gantt Chart, Section 1 (Top Section)

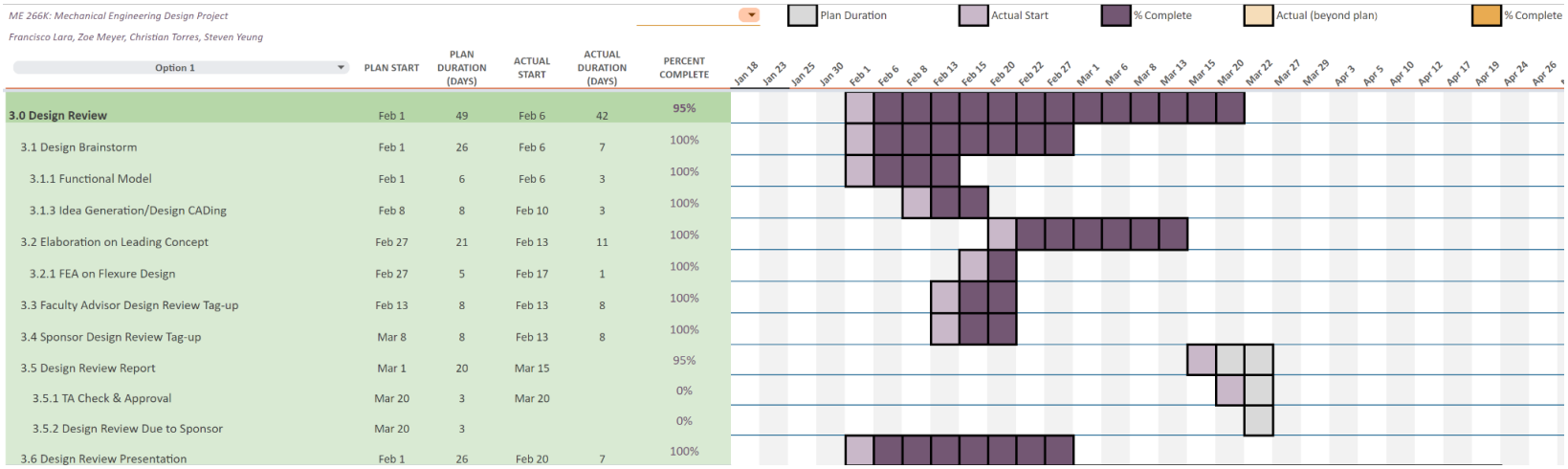

Figure A.2. Gantt Chart, Section 2 (Middle Section)

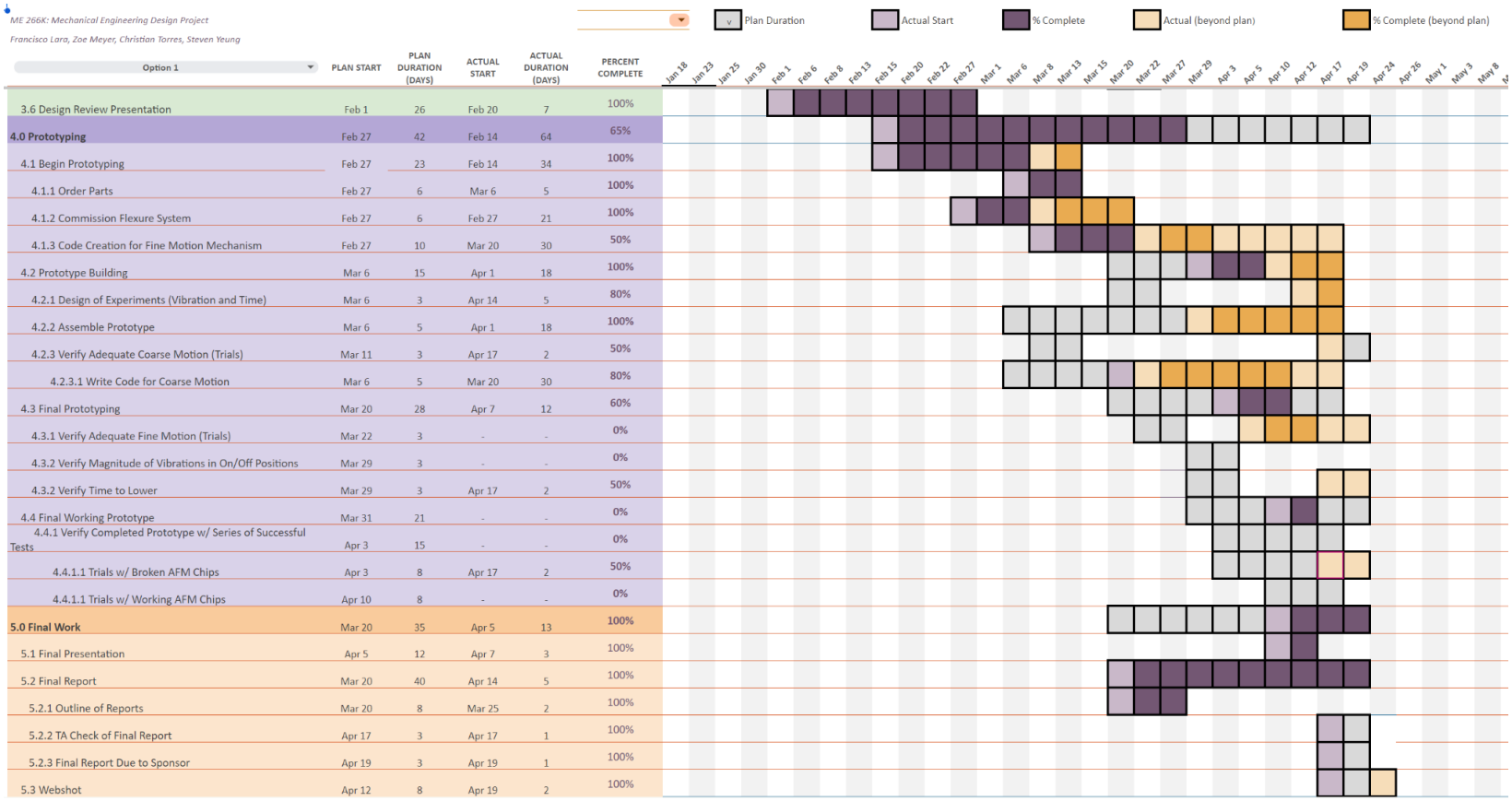

Figure A.3. Gantt Chart, Section 3 (Bottom Section)

APPENDIX B: **FINAL PROTOTYPE PHOTOS**

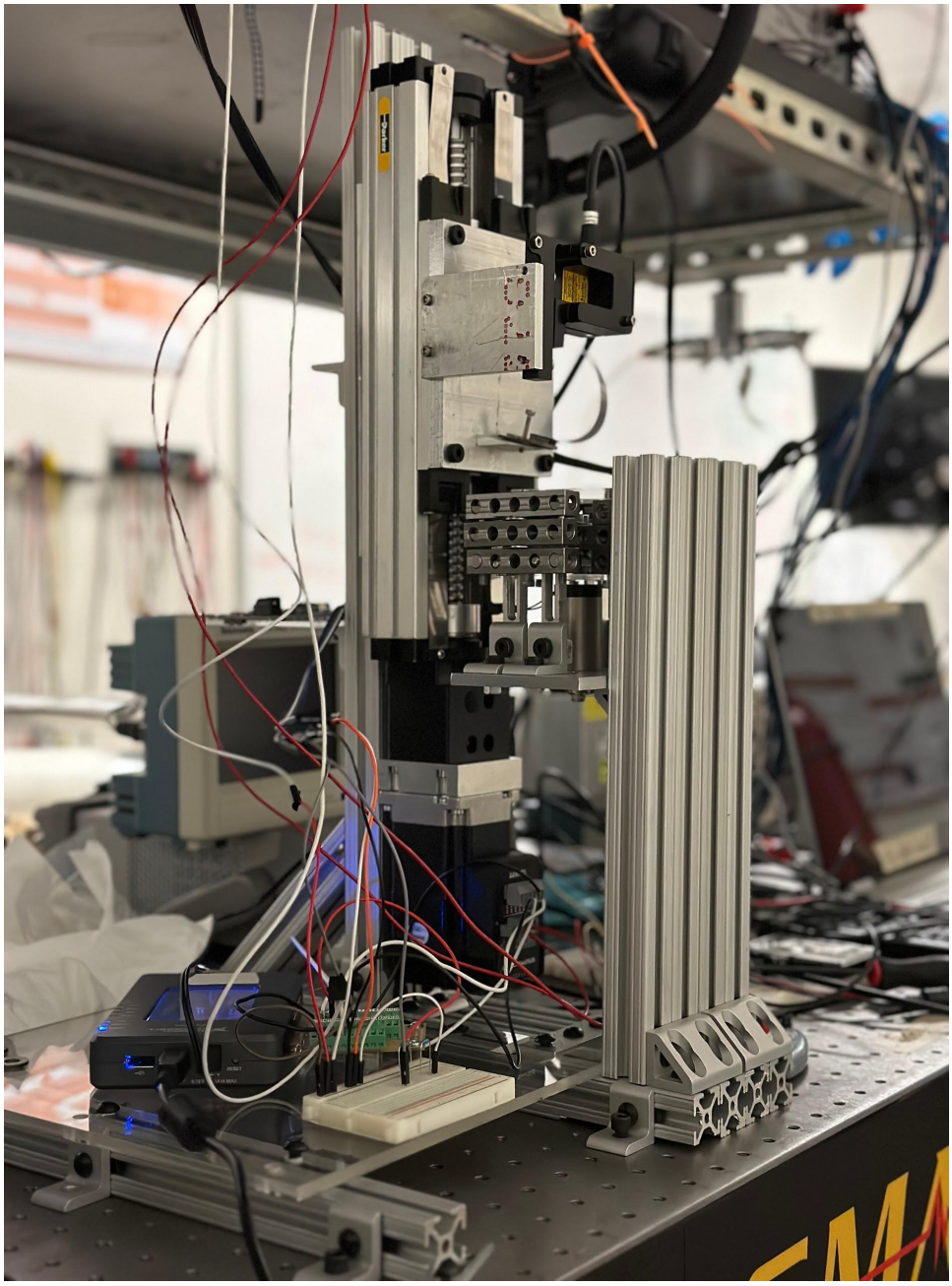

Figure B.1. Bottom Left View of Final Prototype.

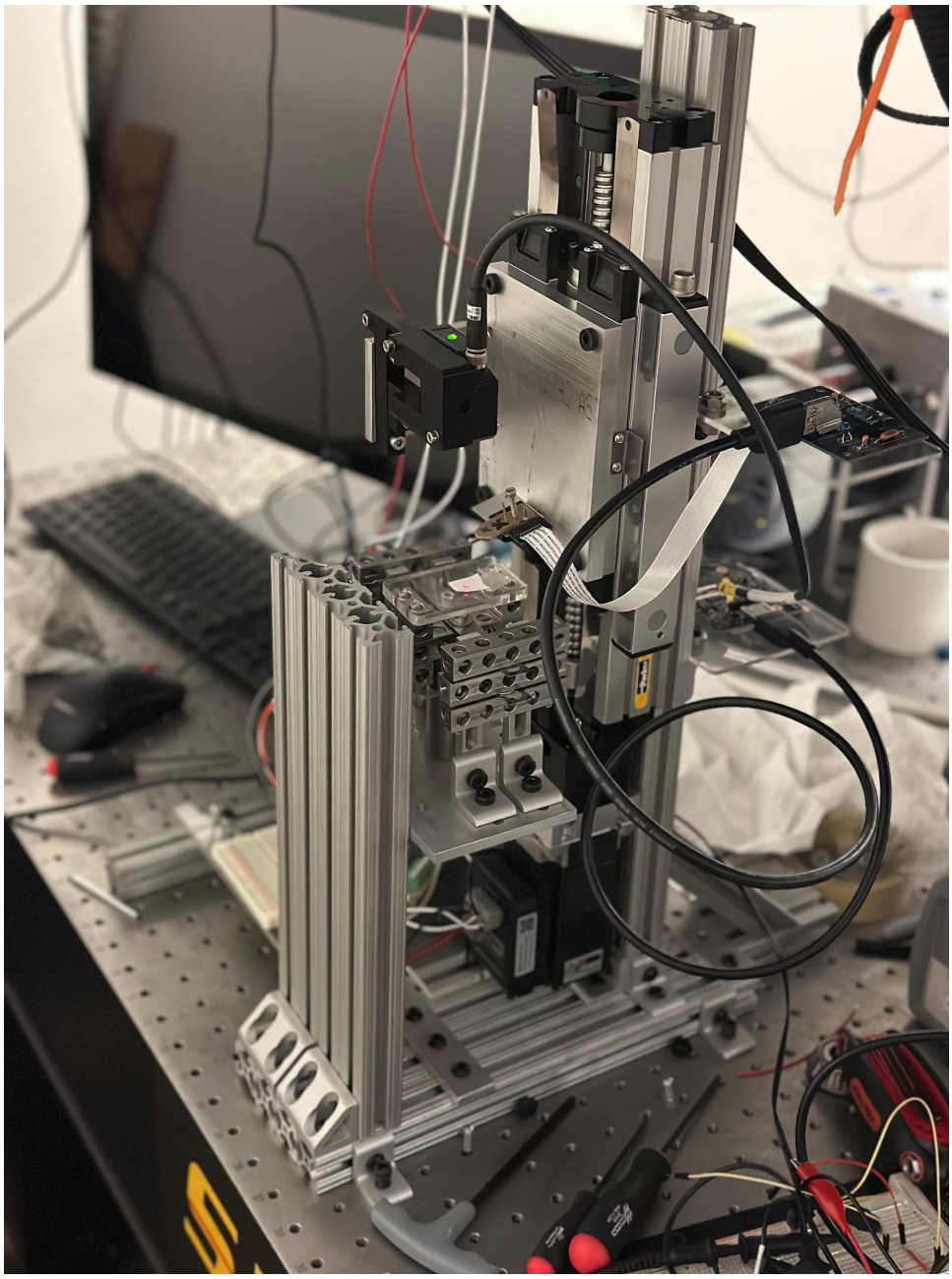

Figure B.2. Top Right View of Final Prototype.

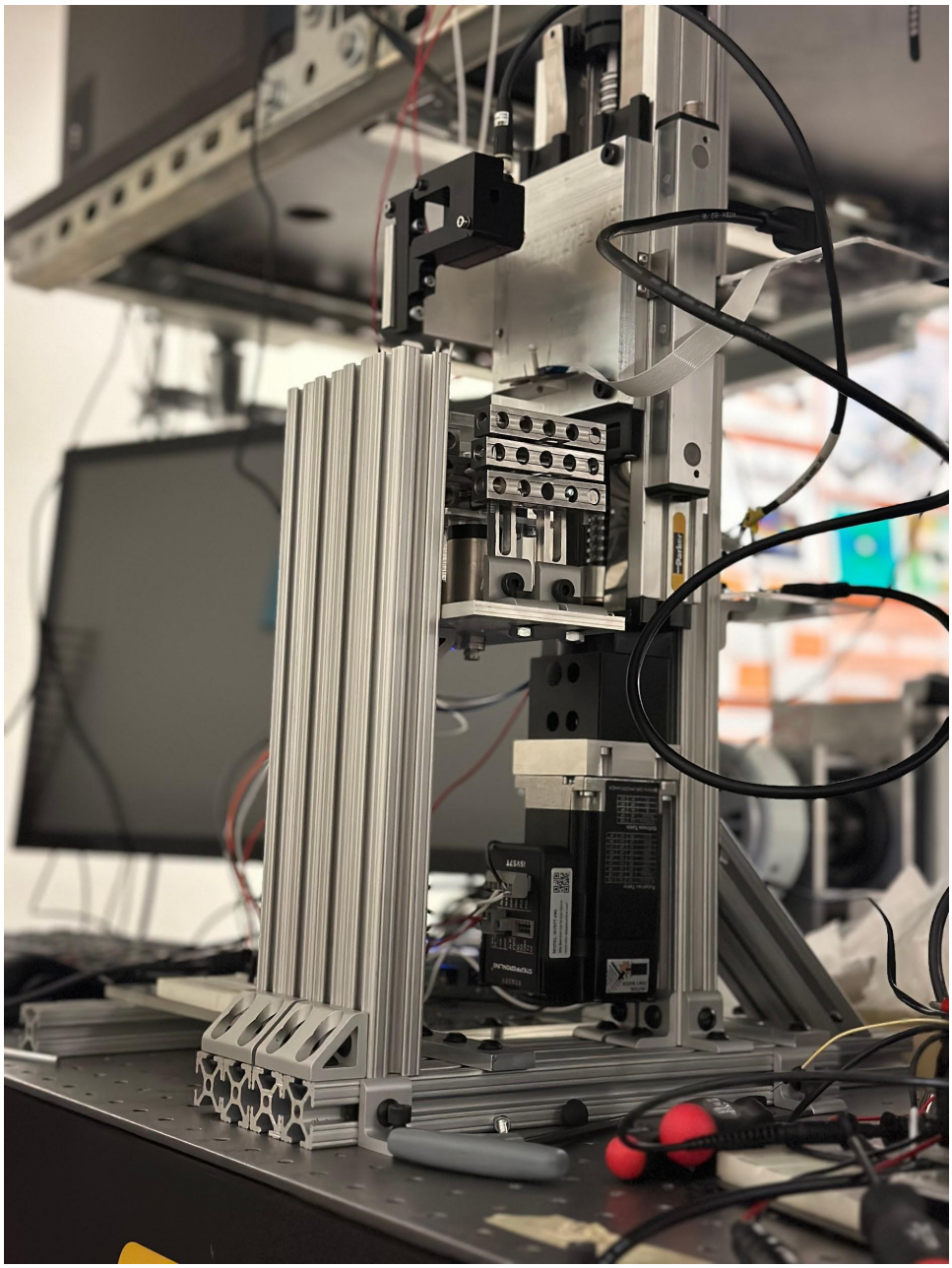

Figure B.3. Bottom Right View of Final Prototype.

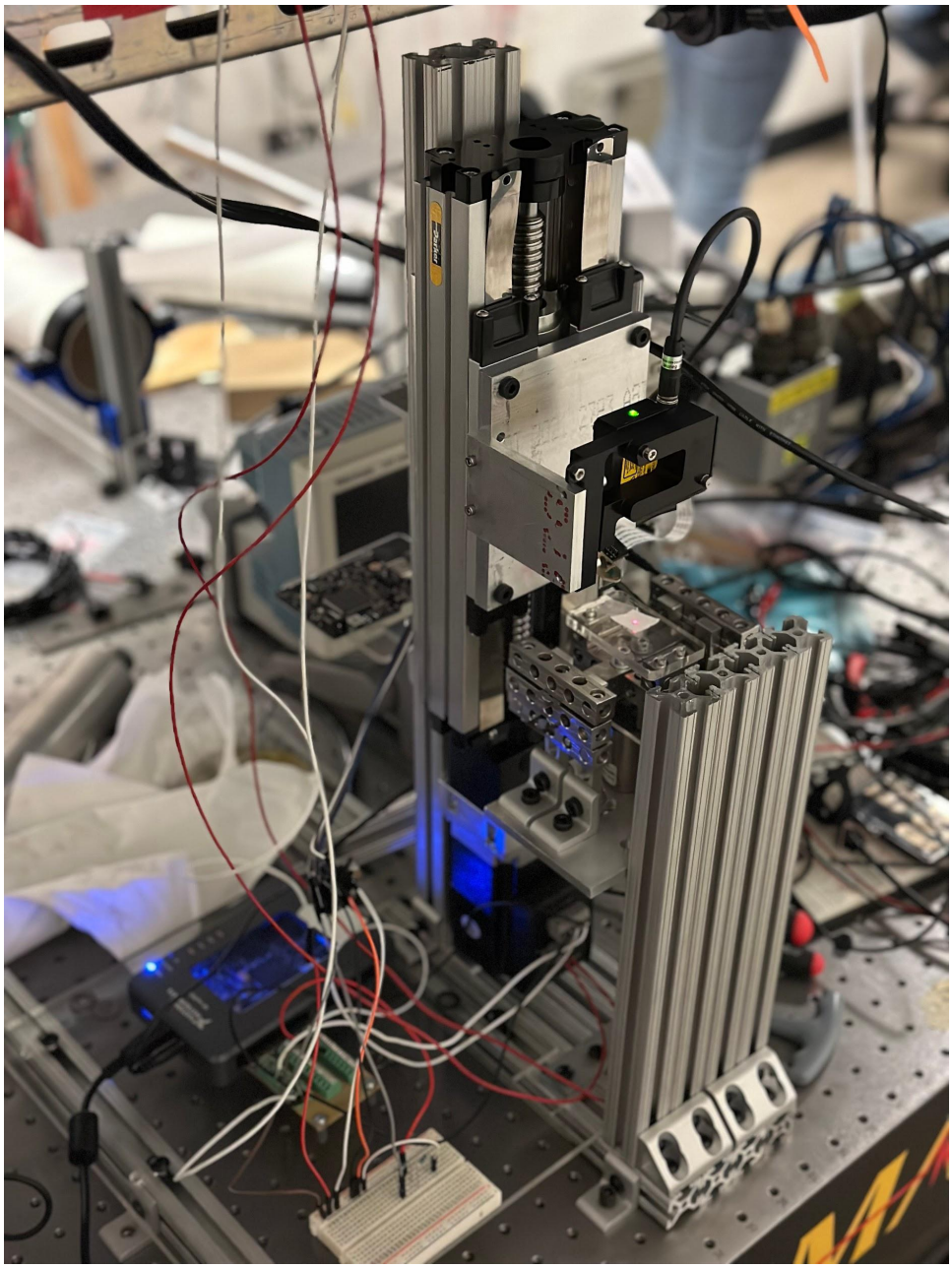

Figure B.4. Top Left View of Final Prototype.

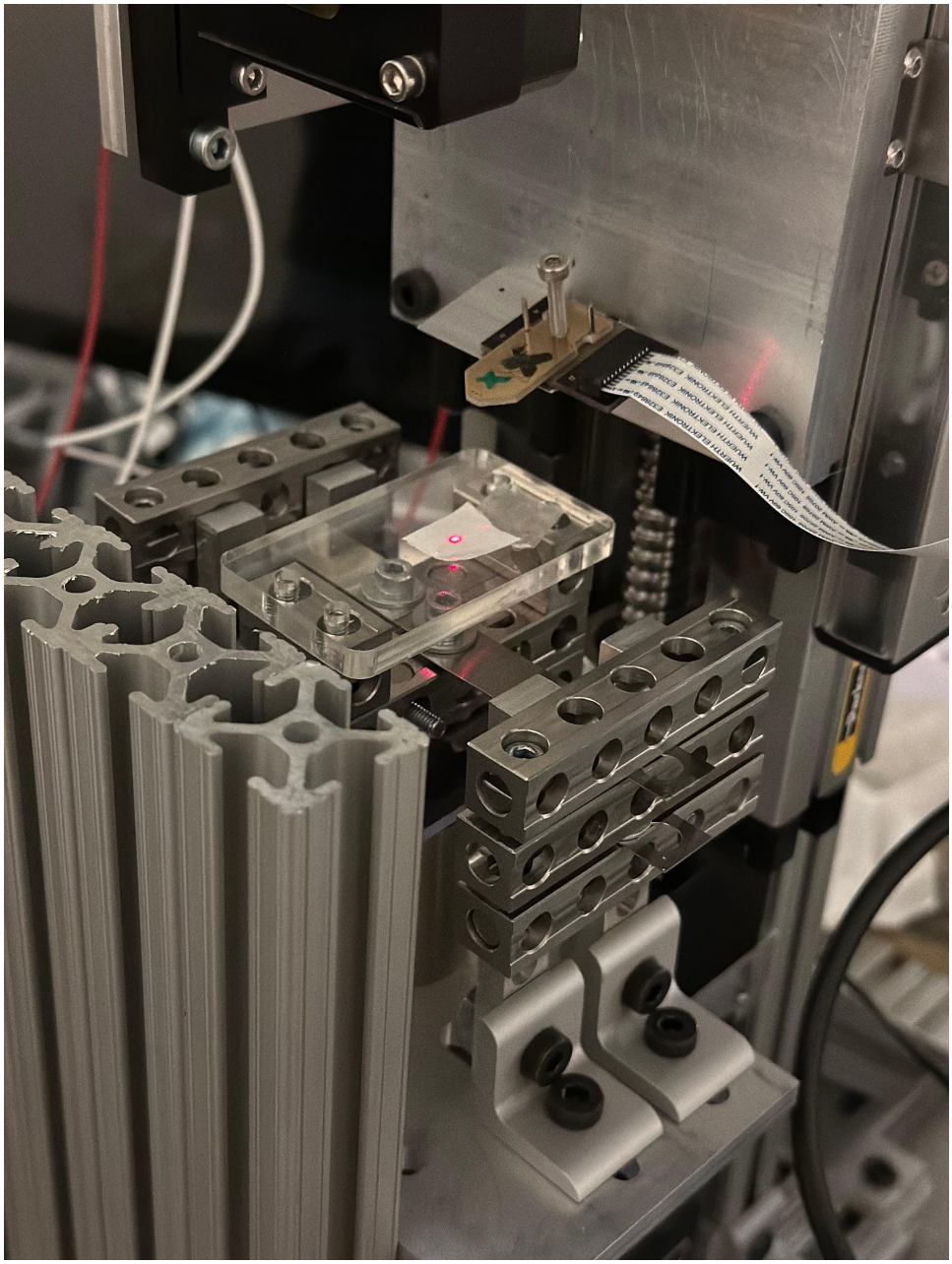

Figure B.5. View of the Sample Stage.

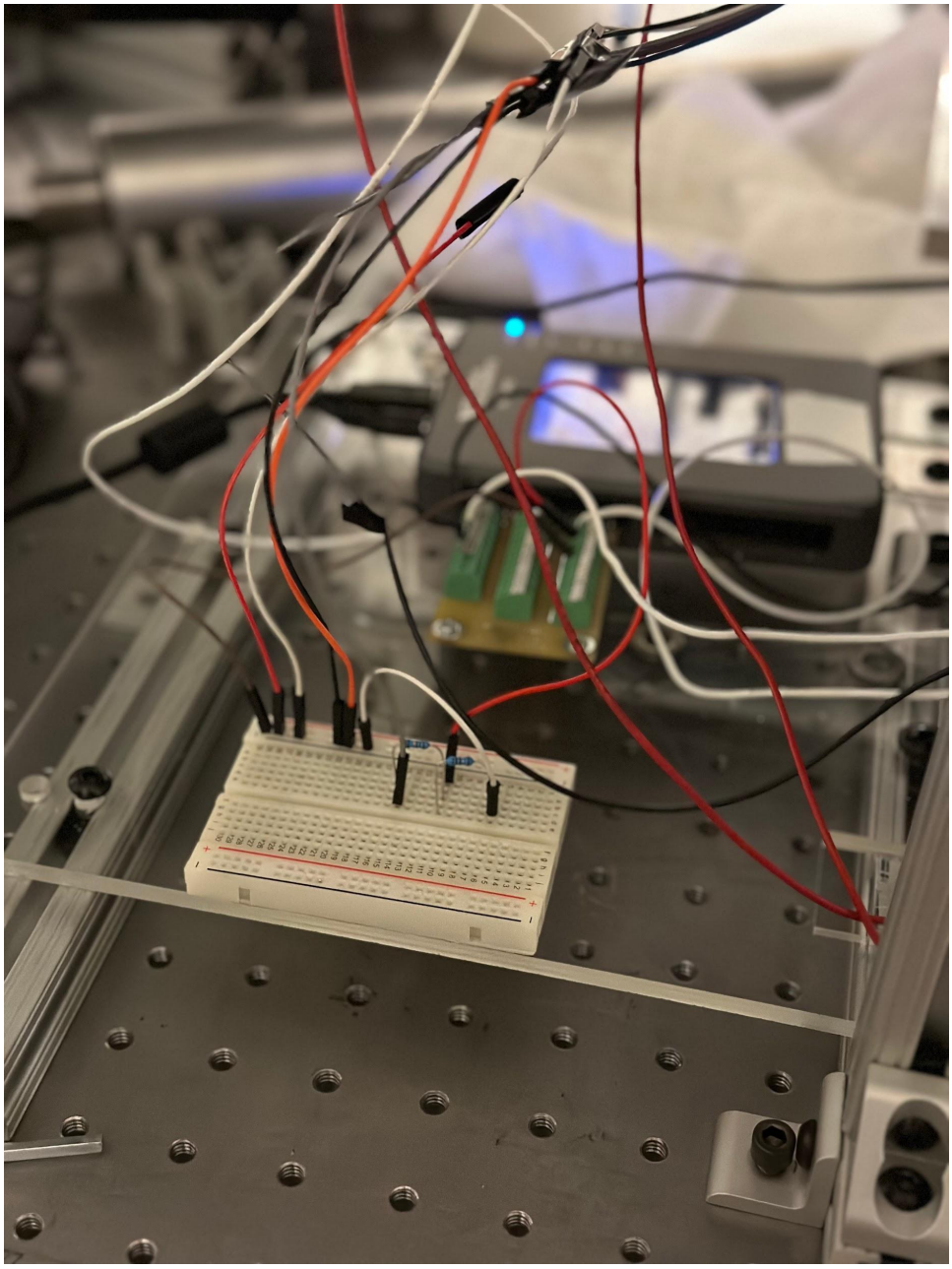

Figure B.6. View of the myRIO and Breadboard.

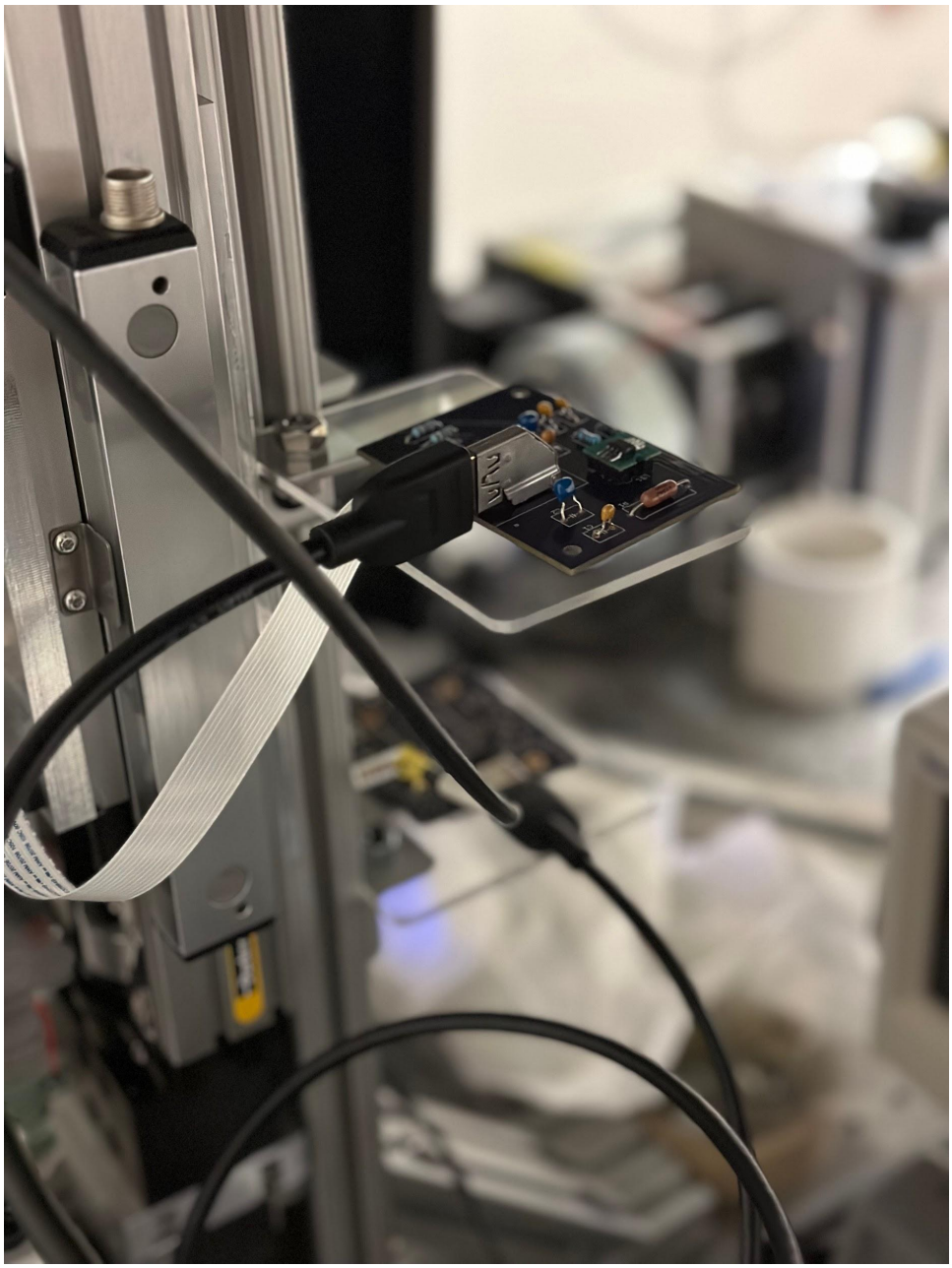

Figure B.7. View of AFM Circuit Board Behind Ball Screw Actuator.

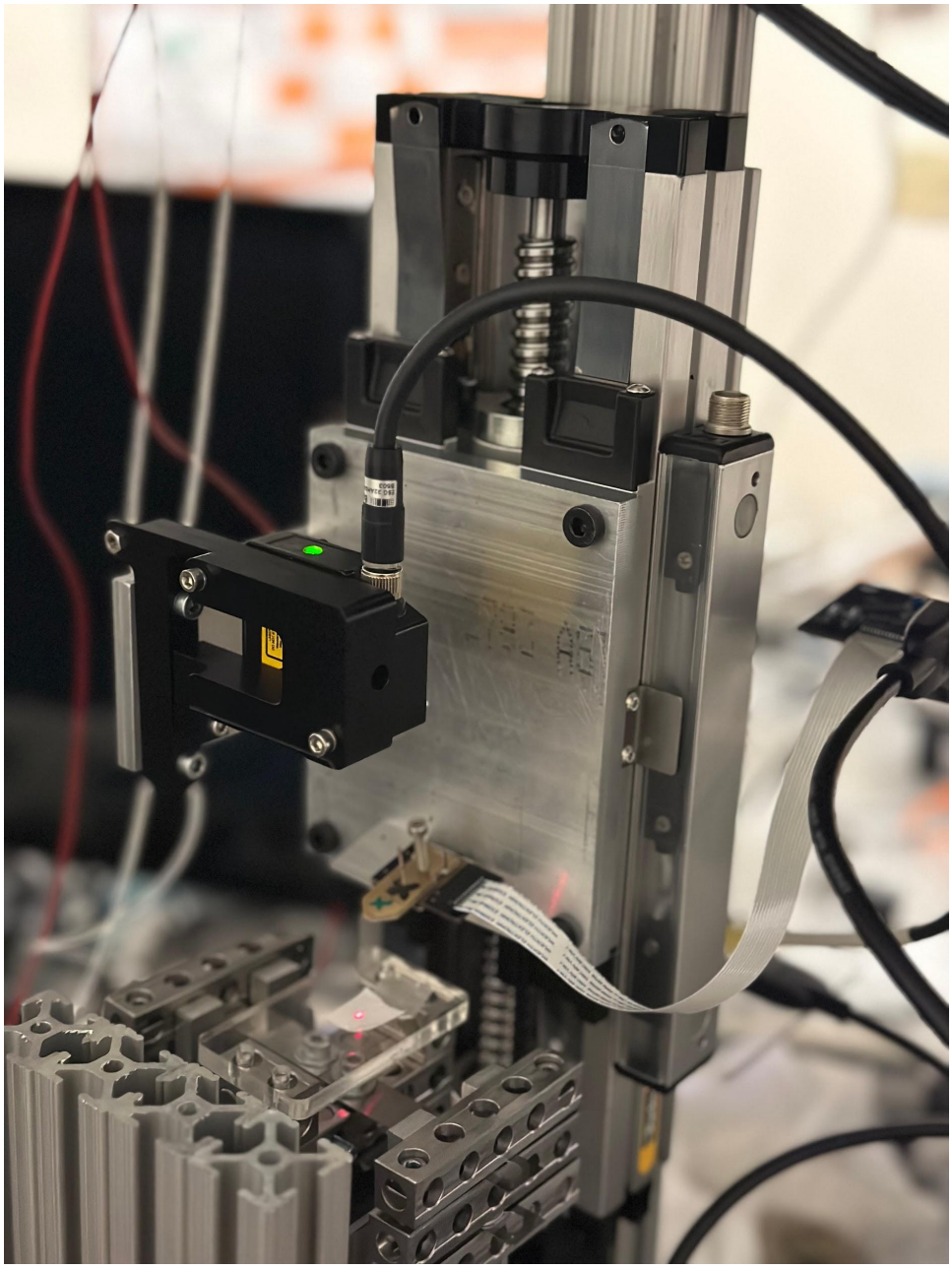

Figure B.8. View of Ball Screw Actuator and Laser Distance Sensor.

APPENDIX C: **HARDWARE INSTALLATION INSTRUCTIONS**

Required Equipment:

- Allen keys compatible with M3, M4, M6 socket head screws
- Level

1. Base Assembly

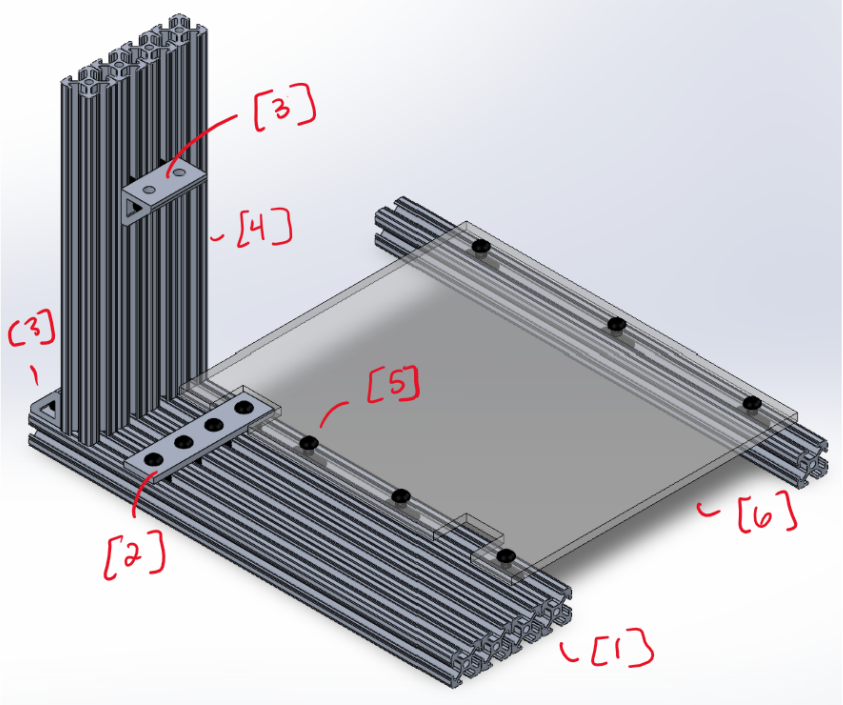

Figure C.1. Base Assembly of Physical Prototype.

Base Assembly Materials:

- 1” 80/20 Aluminum (14” length) (x5) [1]
- 4” Connecting Piece (x1) [2]
- 2” 80/20 Gussets (x3) [3]
- 1” 80/20 Aluminum (10” length) (x4) [4]
- 80/20 Nut and Bolt (x20) [5]

- Acrylic Platform (x1) [6]

Procedure:

1. Connect the 10” and 14” 80/20 pieces utilizing the 2” gussets and 80/20 nuts and bolts to form an ‘L’ shape with the 14” 80/20 being the base. Ensure the edge of the gussets are flush with the end of the 14” 80/20 aluminum and are tightly screwed together.
2. Join the 14” 80/20 together utilizing the 4” connecting piece using the 80/20 nuts and bolts. Do not fully tighten down the connecting piece as it will be moved later.
3. Tighten the final 2” 80/20 gusset to the 2 central 10” 80/20 pieces. Attach the gusset such that a face lies upward as shown in the figure B.1. The vertical distance between the exposed gusset surface and 10” 80/20 should be 50 mm. Use a level to ensure that the gusset lies perfectly flat.
4. Lay the acrylic platform square against the 10” 80/20. Move the 4” connector such that it is aligned with the slot of the acrylic platform.
5. Slide 2 80/20 nuts through the rail on which the acrylic platform sits. Move the nuts such that they are aligned with the acrylic platform holes. Tighten nuts down with 80/20 screws. Leave the third hole empty.
6. Attach the final 14” 80/20 piece to the acrylic platform using 80/20 nuts and bolts.

2. Ball-Screw Actuator

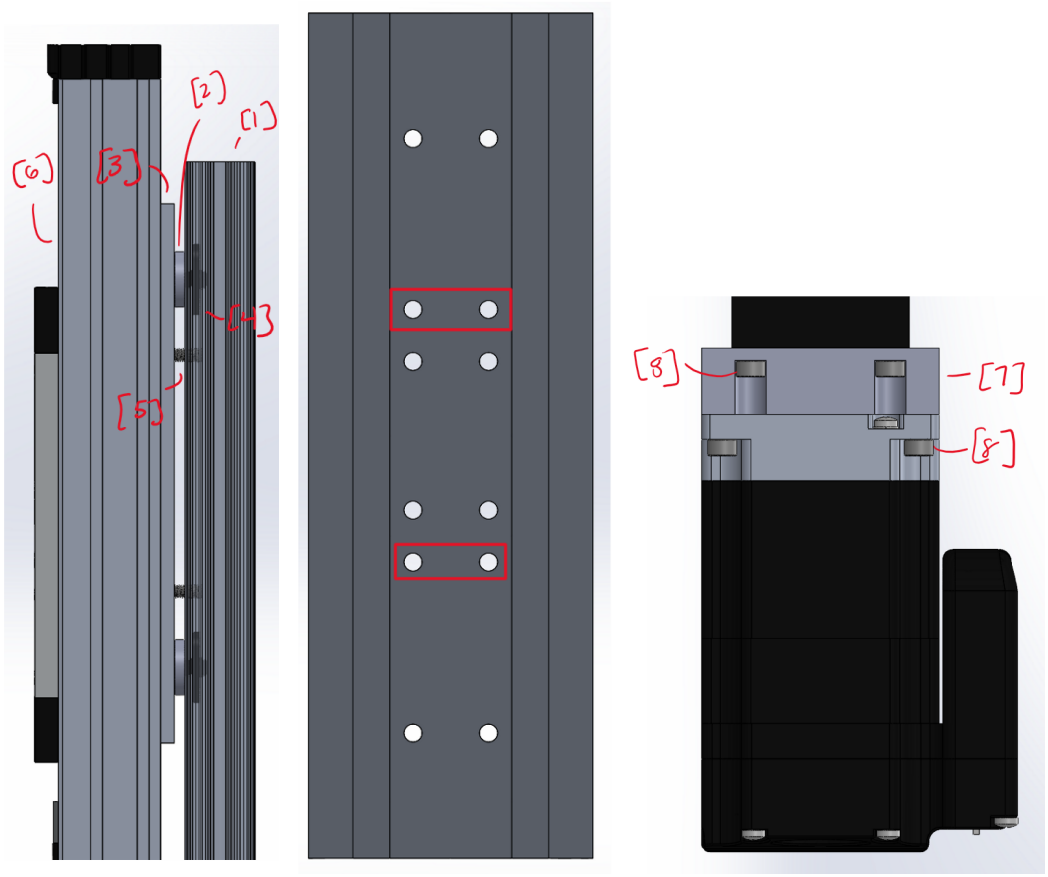

Figure C.2. Ball-Screw Actuator Assembly of Physical Prototype.

Ball-Screw Actuator Materials:

- 1” 80/20 Aluminum (18” length) (x2) [1]
- Washers (x4) [2]
- Spacing Plate (x1) [3]
- 80/20 Nuts and Bolts (x4) [4]
- 10-32 Screws (x4) [5]
- 404xr Ball Screw Actuator (x1) [6]
- M4 Screws (x8) [7]

- Motor Mount (x1) [8]

Procedure:

1. Attach motor mount to ball screw actuator using M4 screws. Attach the servo motor to the motor mount using M4 screws. Ensure the servo motor driver is facing in the same direction as the ball screw actuator (i.e not the back plate of the ball screw).
2. Align and place the two 18” 80/20 together.
3. Place 80/20 screws on the counterbored holes of the spacing plate. On the other side of the spacing place, place washers and 80/20 nuts on each of the 80/20 screws. Slide the 80/20 nuts along the rails of the 18” 80/20 and ensure that the washers remain between the spacing plate and 18” 80/20 as shown in figure B.2.
4. Move the spacing plate along the rail such that the distance between the surface of the base 80/20 and bottom of plate is 245 mm. Tighten the 80/20 screws.
5. Align the holes between the spacing plate and ball screw actuator. Drop and hand tighten 10-32 screws. Actuate the ball screw via motor or physical force to access the other two screw holes. Proceed to fully tighten all 10-32 screws.

3. Ball-Screw to Base

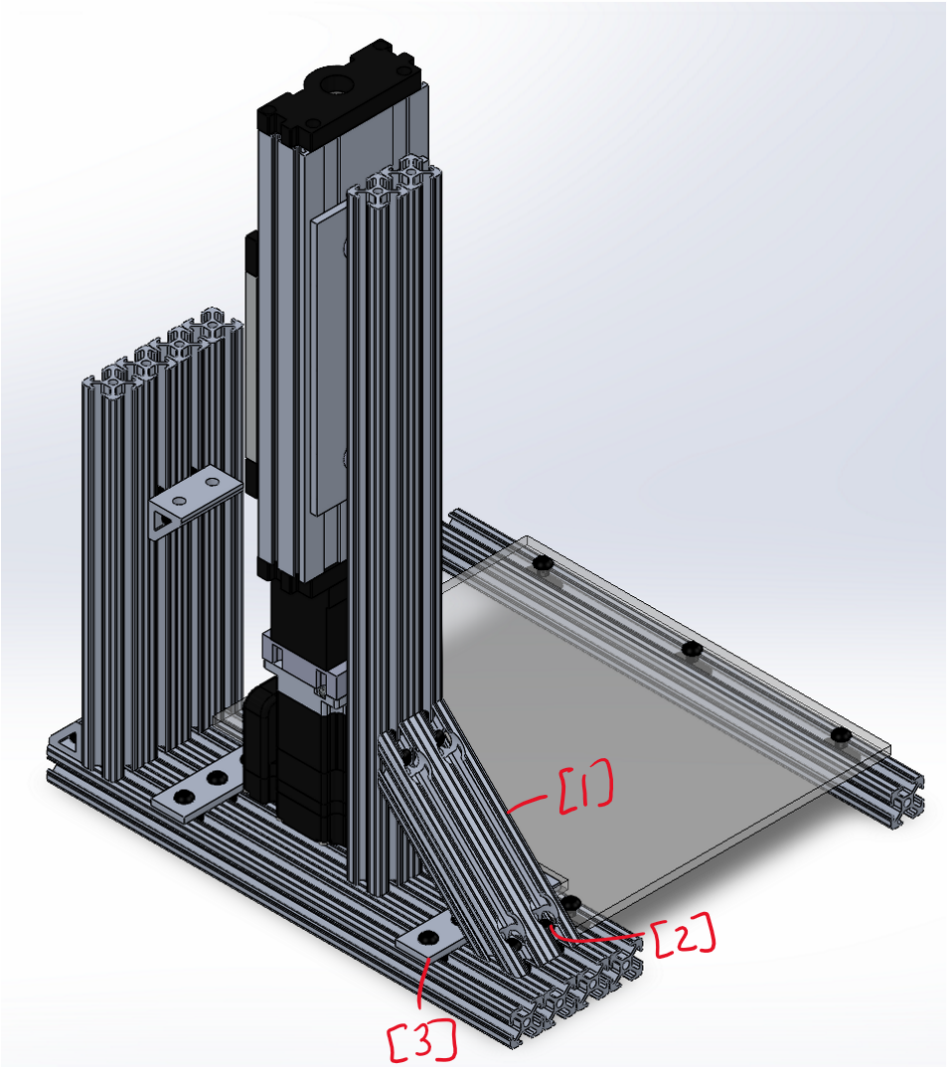

Figure C.3. Ball Screw to Base Assembly of Physical Prototype.

Ball-Screw to Base Materials:

- 1” 80/20 Aluminum Brace (6” Length) (x2) [1]
- 80/20 Nuts and Bolts (x9) [2]
- 4” Connecting Piece (x1) [3]

-

Procedure:

1. Connect the ends of the 80/20 braces to the 18” 80/20 with 80/20 nuts and bolts. Ensure that the flat side of the brace is aligned with the bottom surface of the 18” 80/20.
2. Position the brace such that it is 17.25 mm from the edge of the base as shown in figure B.3.
3. Lay 4” connecting piece on top of base such that it is aligned with the slot of the acrylic platform and underneath the brace. Slide 80/20 nuts into the rails such that they lie below the holes on the 4” connecting piece. Tighten connecting piece to base with 80/20 screws.
4. Slide 80/20 nuts into place and screw braces to base. In addition, add the missing 80/20 screw and nut to the last hole of the acrylic platform.

4. Ball-Screw Mounts

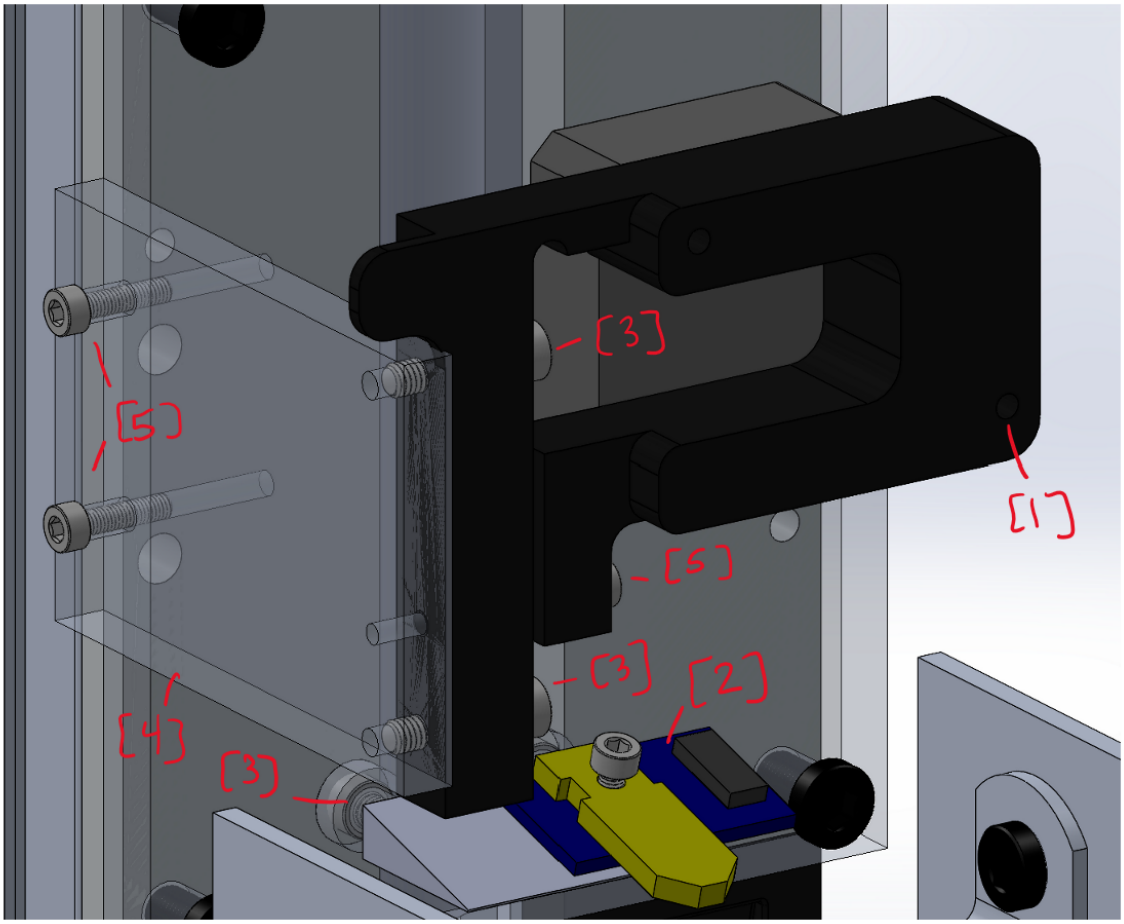

Figure C.4. Ball-Screw Mounts Assembly of Physical Prototype.

Ball-Screw Mounts Materials:

- Laser (x1) [1]
- AFM and Piezoscanner (x1) [2]
- M4 Screws (x4) [3]
- Laser Mounting Plate (x1) [4]
- M3 Screws (x4) [5]

Procedure:

1. Attach laser mounting plate to the plate attachment with M3 screws as shown in figure B.4.
2. Attach the AFM to the piezo scanner and angled piece by lining up the pin holes and using an M3 screw. Then, attach the angled piece to the plate attachment using the counterbored hole.
3. Attach mounting plate to ball screw actuator as shown in figure B.4 utilizing M6 screws.
4. Attach the laser to the laser mounting plate with M3 and M4 screws as shown in figure B.4. Ensure the laser is aligned correctly. The angular position of the laser can be slightly varied by tightening or loosening the M3 screw.

5. Flexure and Voice Coil Structure

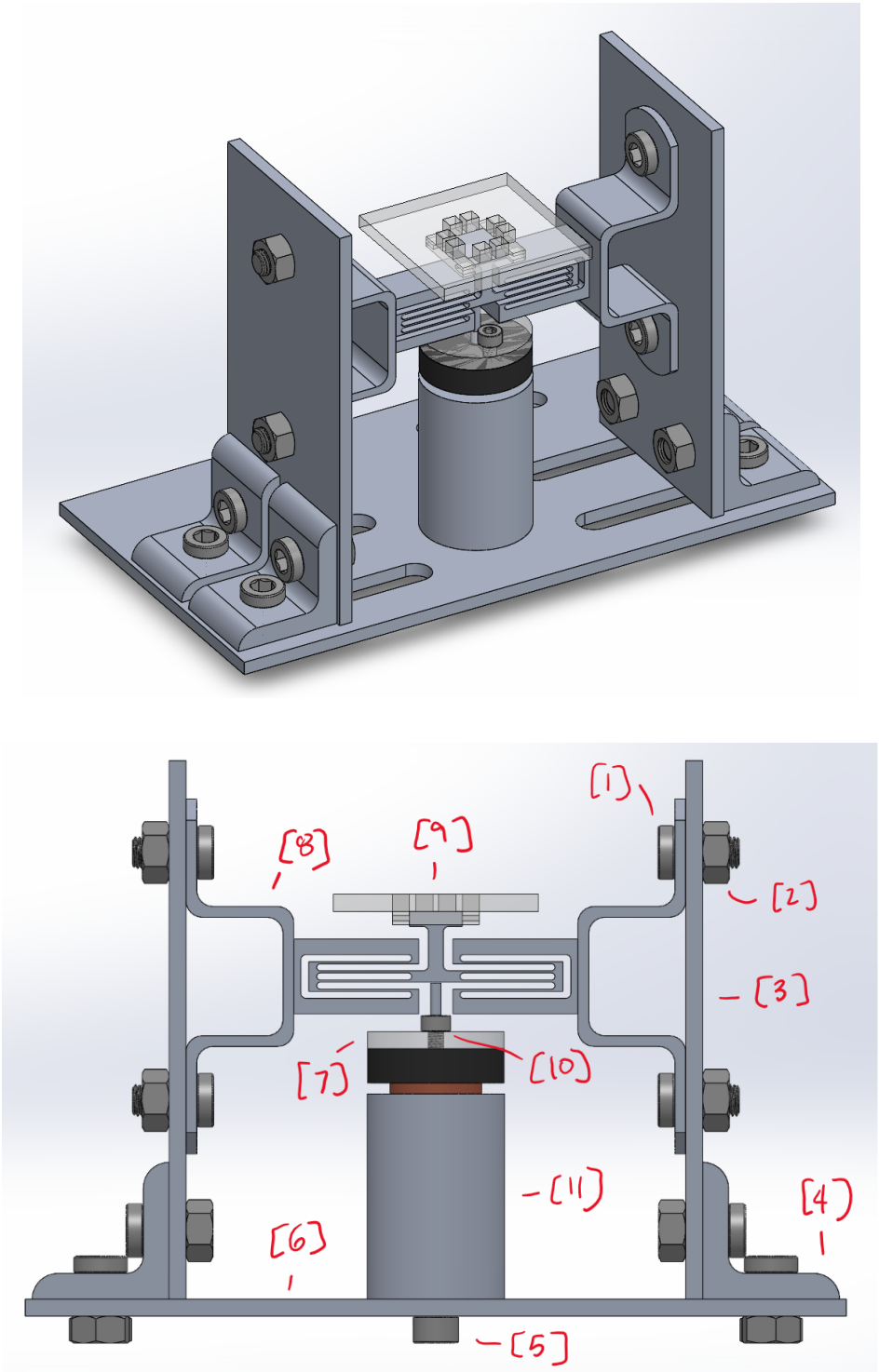

Figure C.5. Flexure and Voice Coil Assembly

Flexure and Voice Coil Structure Materials:

- M6 Screws (x12) [1]
- M6 Nuts (x12) [2]
- Bracket Plate (x1) [3]
- 80/20 L Brackets (x4) [4]
- M5 Screw (x1) [5]
- Voice Coil Plate (x1) [6]
- Voice Coil Attachment (x1) [7]
- U Brackets (x2) [8]
- Flexure Sample Stage (x1) [9]
- M3 Screws (x2) [10]
- Voice Coil (x1) [11]
- Loctite

Procedure:

1. Screw the U brackets into each of the bracket plates using appropriate screws and nuts (M6 screws should function for this case).
2. Attach the flexure to the U brackets utilizing loctite. Ensure the flexure is centered both vertical and horizontally on the U brackets.
3. Attach the L brackets to the bracket plates utilizing M6 screws and nuts. Do not fully tighten.
4. Attach voice coil to the voice coil plate utilizing an M5 screw. Attach voice coil attachment to voice coil using M3 screws.

5. Attach the L bracket - bracket plate structure to the voice coil plate using M6 screws and nuts. Ensure the structure centered on top of the voice coil attachment.

6. Flexure and Voice Coil Structure to Frame

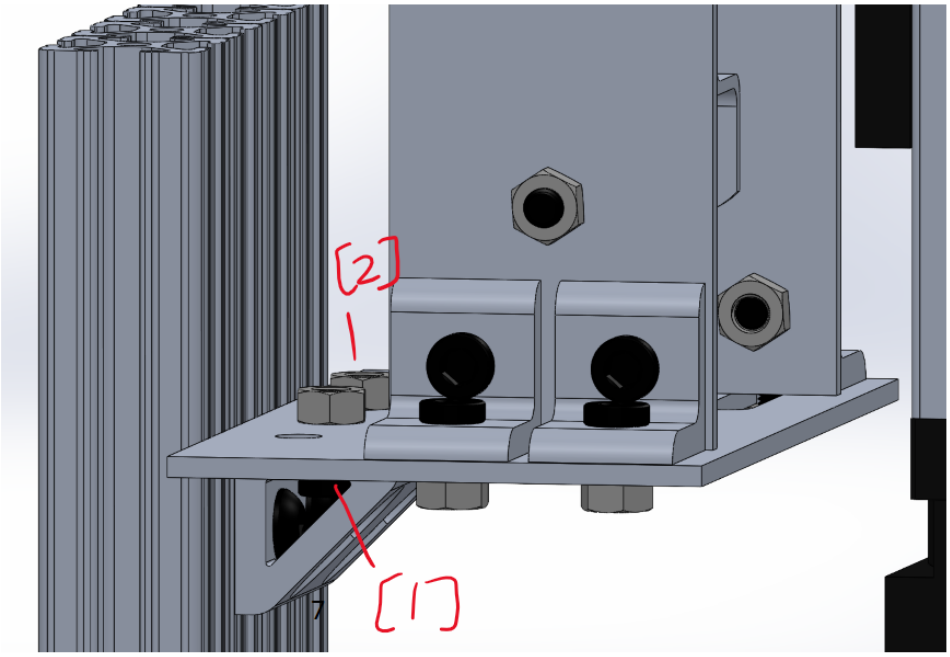

Figure C.6. Flexure and Voice Coil Structure to Frame

Flexure and Voice Coil Structure to Frame Materials:

- M6 Screw (x2) [1]
- M6 Nuts (x2) [2]

Procedure:

1. Attach the structure constructed in ‘Flexure and Voice Coil’ to the overall frame utilizing 80/20 nuts and bolts and M6 screws and nuts.

7. AFM Acrylic Platforms

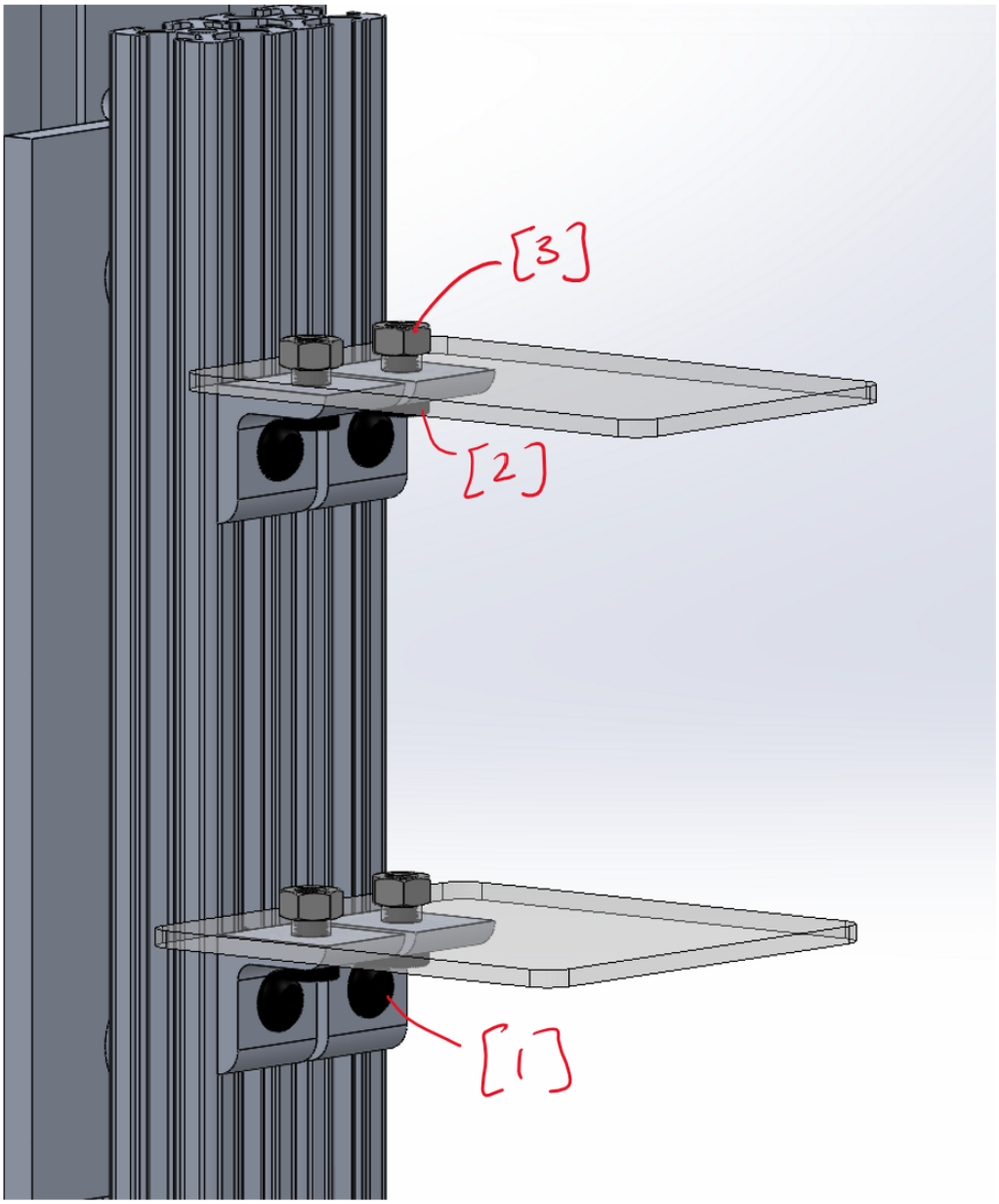

Figure C.7. AFM Acrylic Platforms

AFM Acrylic PlatformsMaterials:

- 80/20 Nuts and Bolts (x4) [1]
- M6 Screws (x4) [2]
- M6 Nuts (x4) [3]
- AFM Acrylic Firmware Board Holder (x1) [4]
- AFM Acrylic Board Holder (x1) [5]
- 80/20 L Brackets (x4) [6]

Procedure:

1. Attach both acrylic boards to the backside of the 18” 80/20 using 80/20 nuts and bolts and M6 hardware as shown in figure B.7 above.
2. The final structure should look like figure B.8 below.

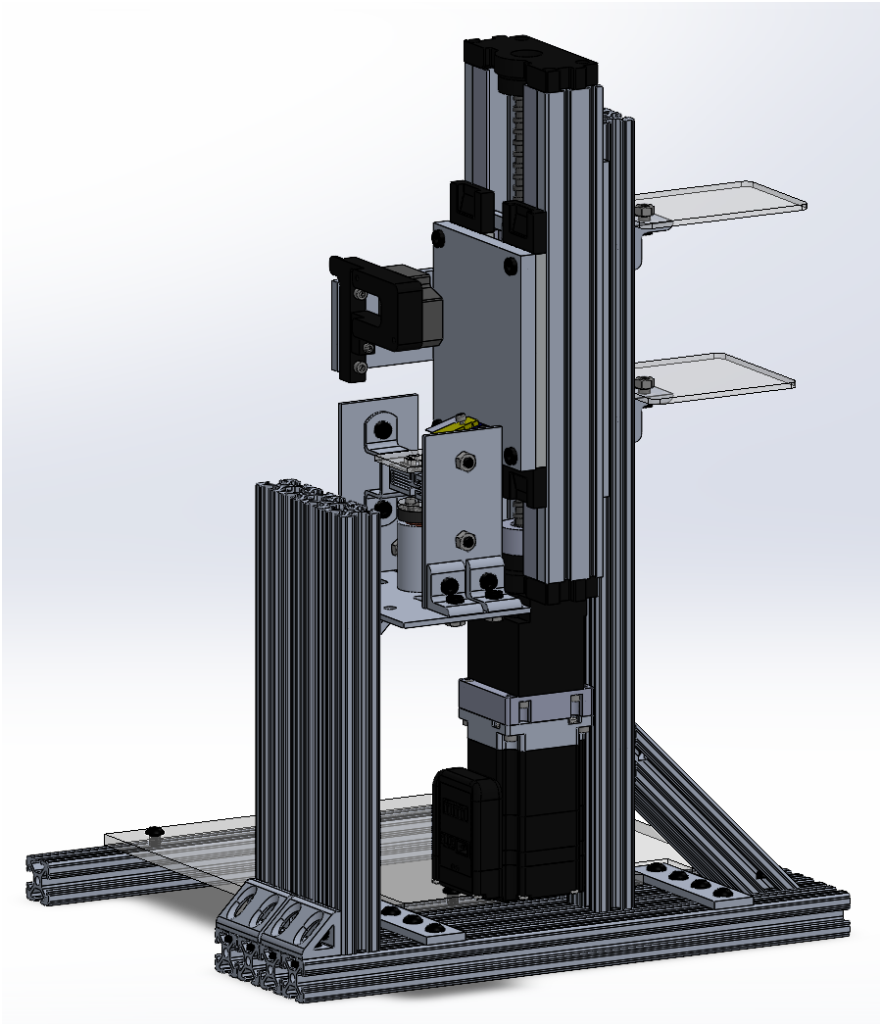

Figure C.8. Completed Physical Assembly

APPENDIX D: **LABVIEW CODE**

The commented LabVIEW code for the automated tip lowering program is as shown below. The code pertaining to the voice coil movement is preliminary and incomplete and is shown only for reference. Due to the size of the code, it has been split into Figures D.1 - D.3 as shown below.

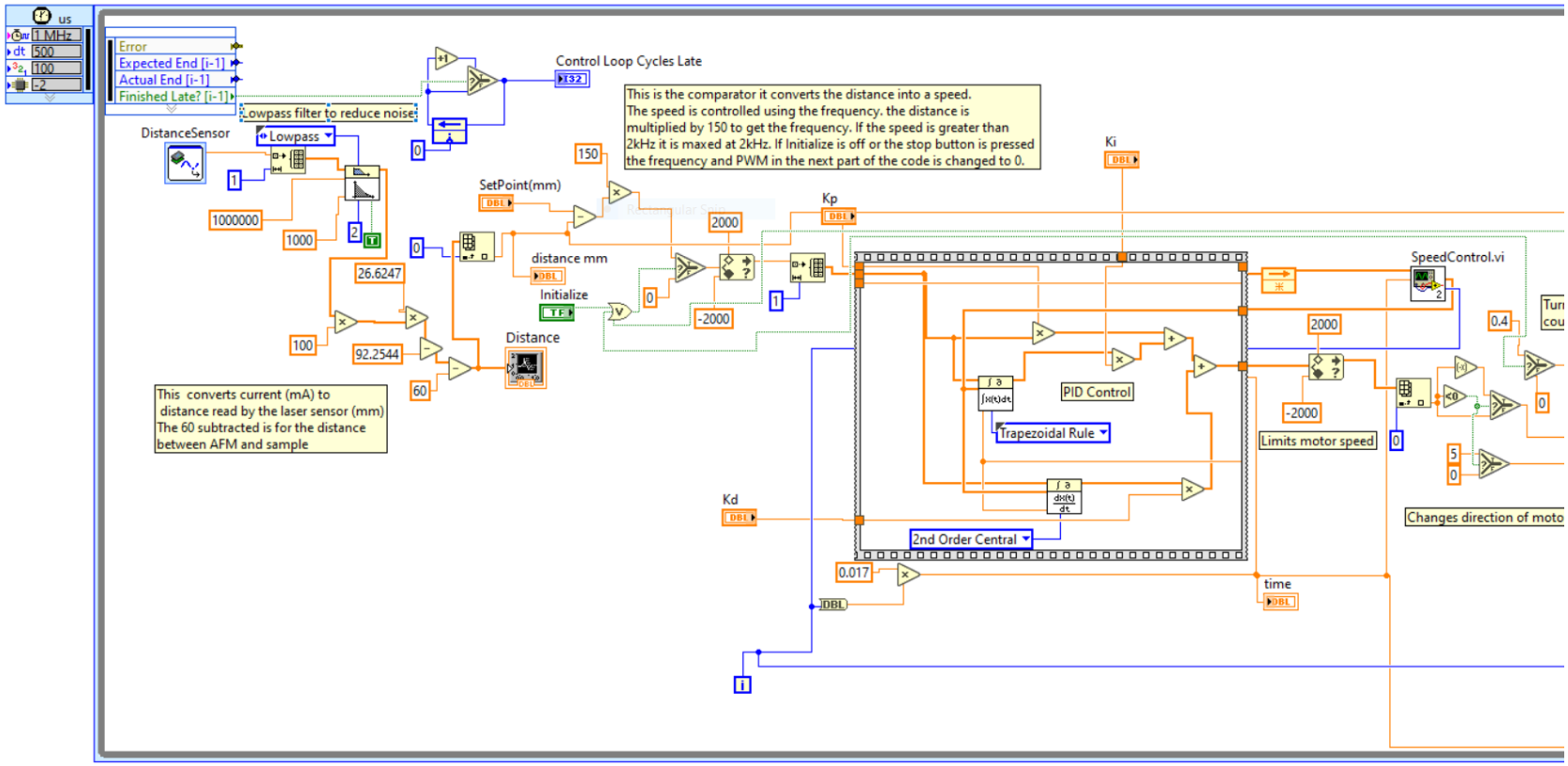

Figure D.1. LabVIEW, Part 1 (Left Section).

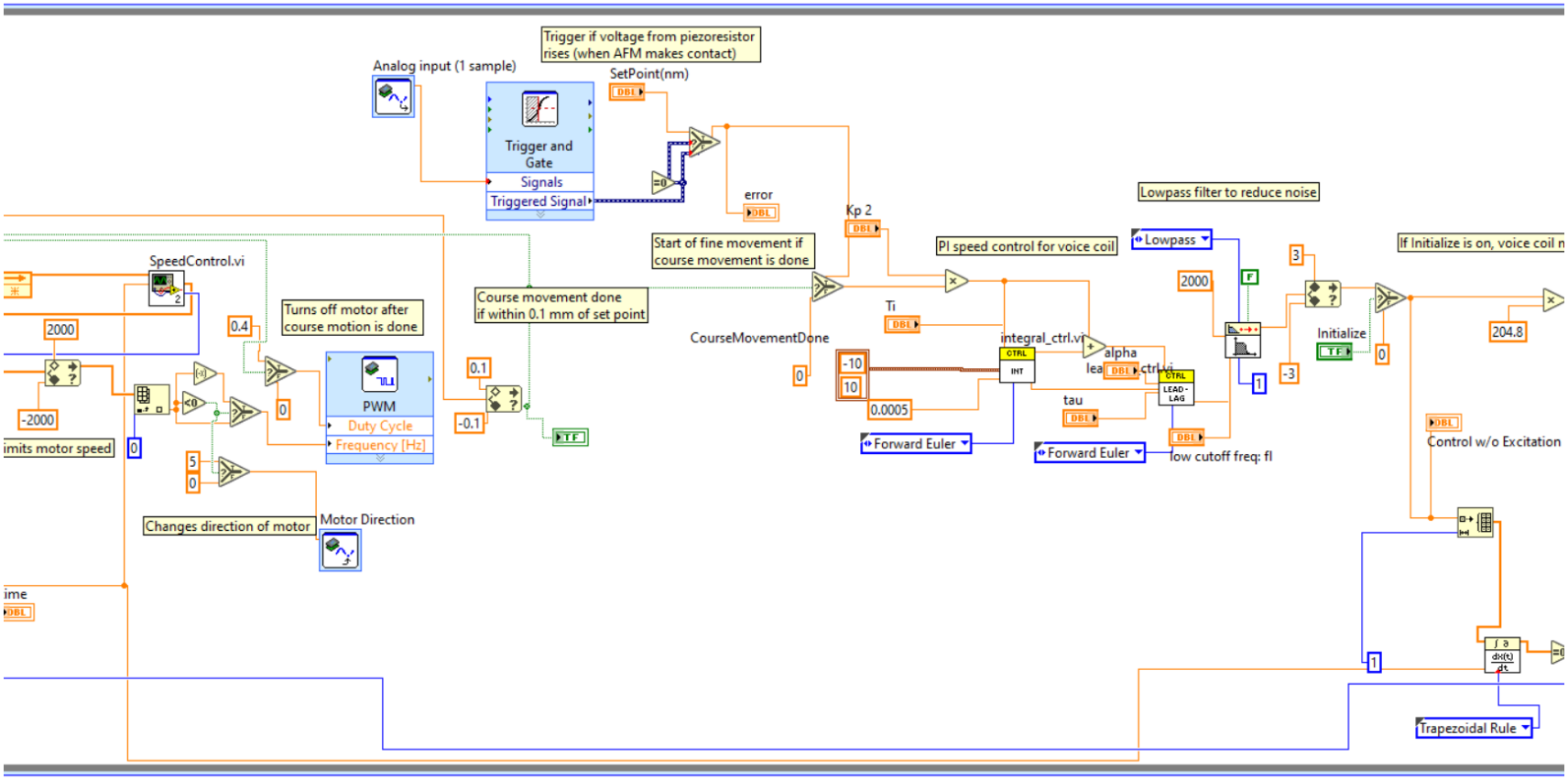

Figure D.2. LabVIEW, Part 2 (Middle Section).

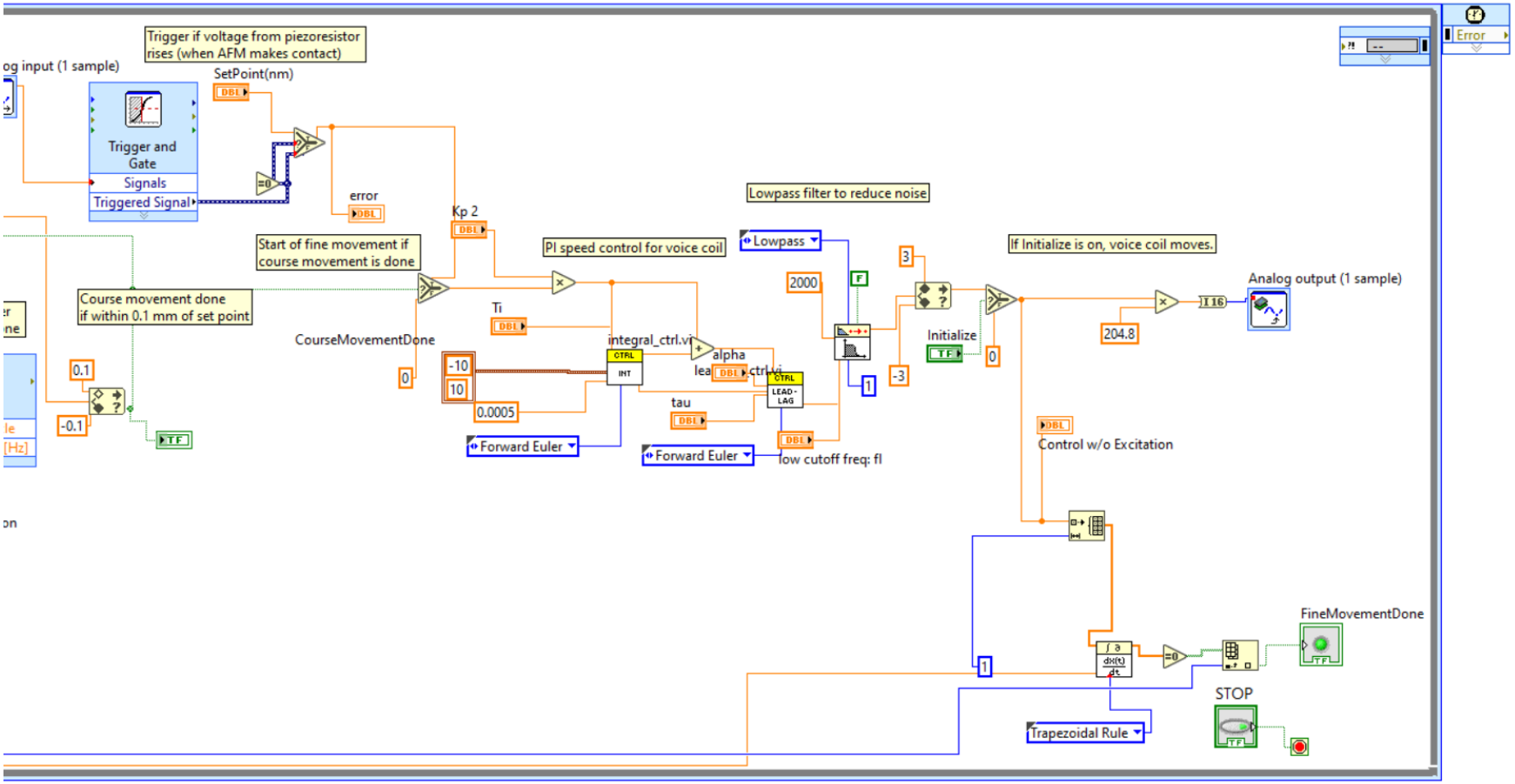

Figure D.3. LabVIEW, Part 3 (Right Section).

APPENDIX E: **ELECTRICAL DIAGRAM**

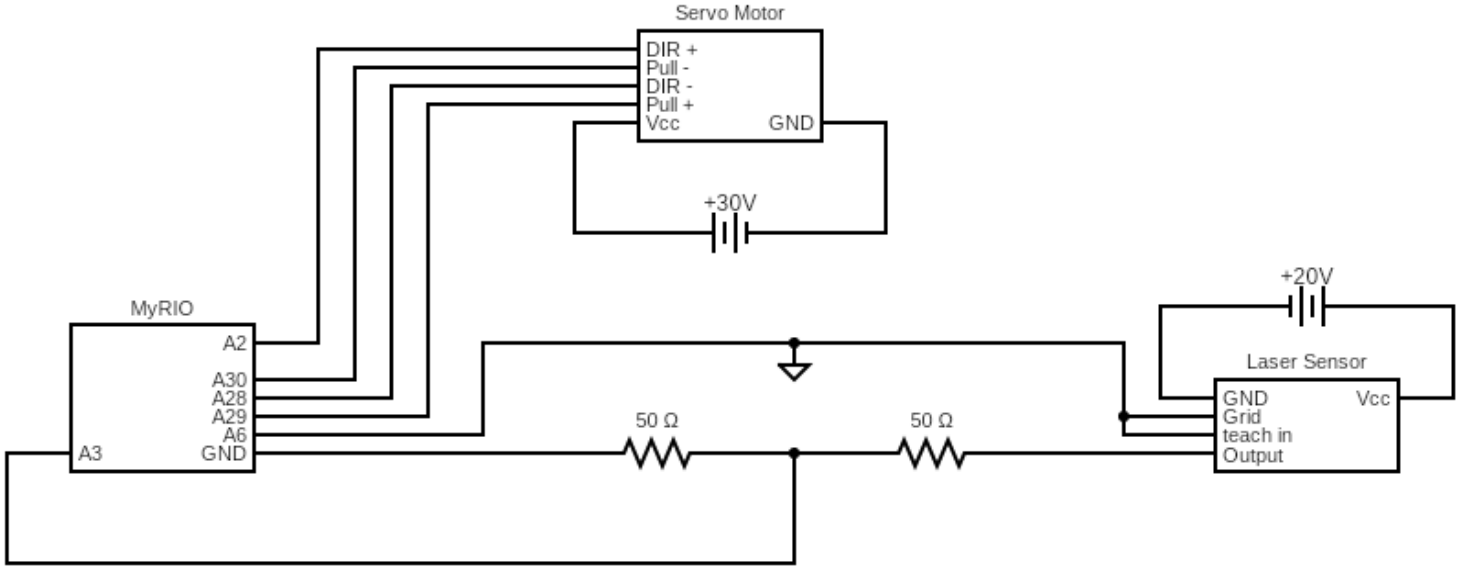

Figure E.1. Circuit Diagram with Servo Motor and Laser Distance Sensor.

APPENDIX F: VOICE COIL-FLEXURE SYSTEM PID CONTROLLER

The voice coil and flexure system PID controller for a mass-spring-damper system our team assembled is shown in this section. System parameters m and k can be pulled from the SolidWorks simulation, but b is more difficult to determine without completing a system ID. For the purposes of this appendix, a b parameter of 0.01 is assumed, corresponding to a lightly damped system. The code shown in Figure F.1 creates the Bode Plot shown in Figure F.2 and pulls up the MATLAB PID tuner app shown in Figure F.3.

```
clc; clear all

% System Parameters
m = .18; %kg
k = 20.165; %N/mm
b = 0.01;

% Transfer Function
s = tf('s')
P = 1/(m*s^2+b*s+k)


% Plot of Transfer Function
%step(P)
bode(P,{1,100})

% pid coefficients
kp = 0.01;
ki = 0.01;
kd = 0.01;

% Modified Transfer Function
Gc = pid(kp, ki, kd);
GcI = feedback(Gc*P, 1);
t = 0:0.01:2
%step(GcI, t)

%opts = pidtuneOptions('CrossoverFrequency',32,'PhaseMargin',90);
%[Gc, info] = pidtune(P, 'pid', opts)

%visualize
pidTuner(P,Gc)
```

Figure F.1. MATLAB Code for Automated PID Controller.

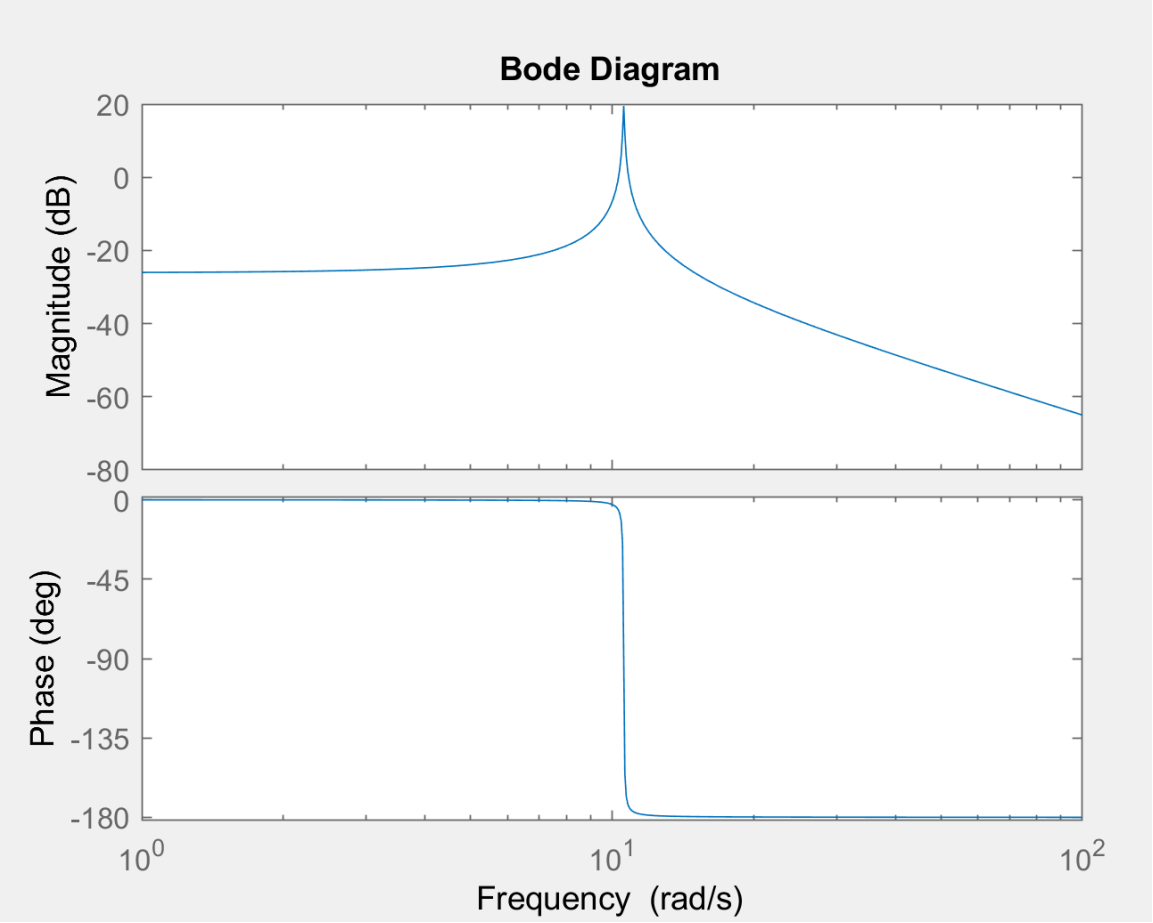

Figure F.2. Resulting Bode Plot for Mass-Spring-Damper.

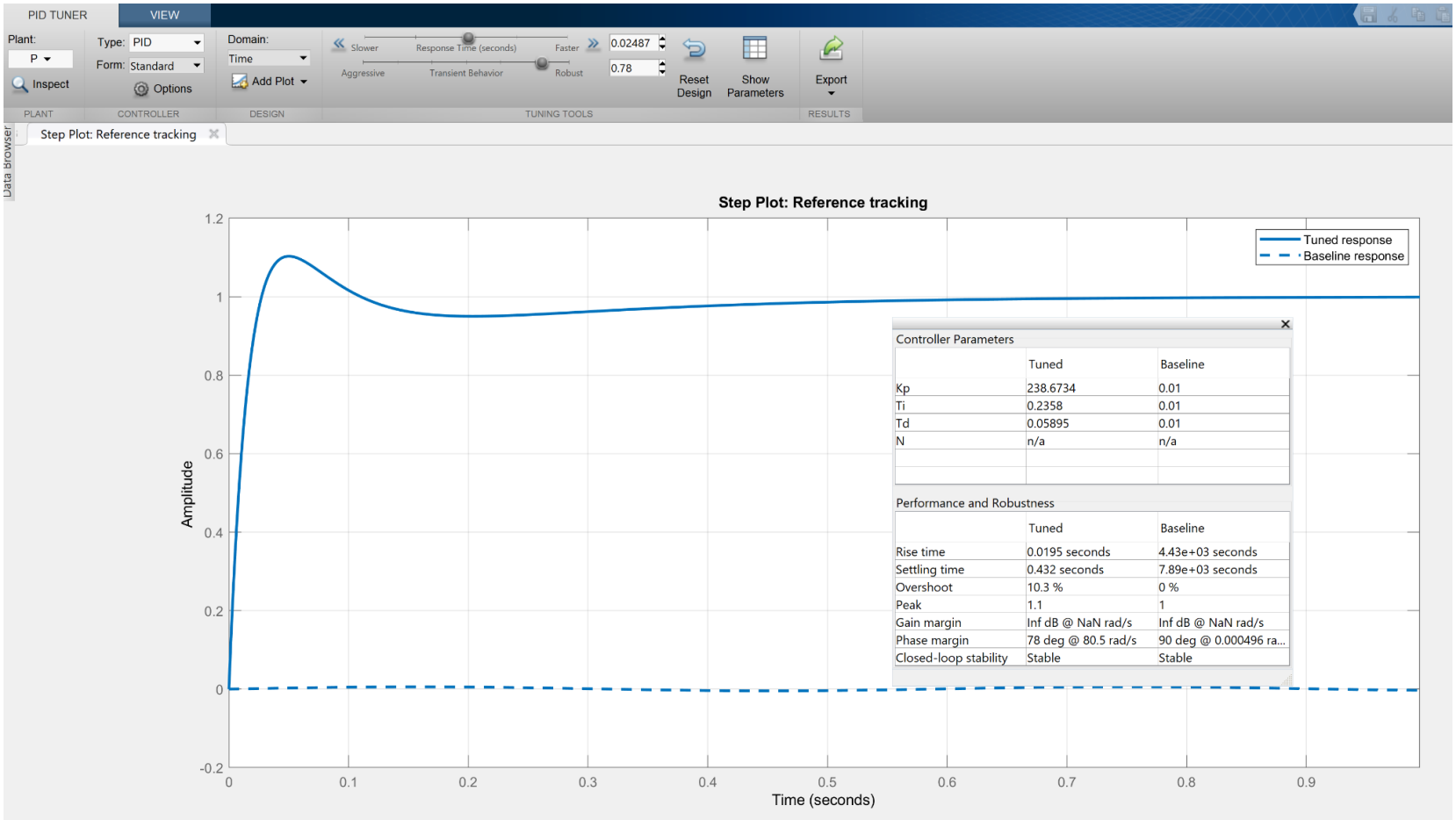

Figure F.3. PID Tuner App for Voice Coil and Flexure System.

The shape of the tuned response in Figure F.3 may be altered using the scroll bars at the top of the app to change the response time and the transient behavior. A slower, more robust response corresponds to a smoother tracked response that has little or no overshoot.